Prediction of Fuel Cladding Performance for Ultra-long Cycle Fast Reactor Application

Ju Ang Jung

Nuclear Science & Engineering Program

Graduate school of UNIST

2012

Prediction of Fuel Cladding Performance for Ultra-long Cycle Fast Reactor Application

Ju Ang Jung

Nuclear Science & Engineering Program

Graduate school of UNIST

Prediction of Fuel Cladding Performance for Ultra-long Cycle Fast Reactor Application

A thesis
submitted to the Graduate School of UNIST
in partial fulfillment of the
requirements for the degree of
Master of Science

Ju Ang Jung

07.23. 2012
Approved by

Major Advisor
Ji Hyun Kim

Prediction of Fuel Cladding Performance for Ultra-long Cycle Fast Reactor Application

Ju Ang Jung

This certifies that the thesis of Ju Ang Jung is approved.

07.23. 2012

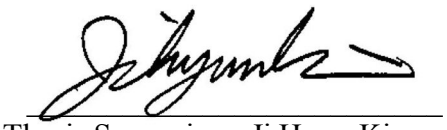

Thesis Supervisor: Ji Hyun Kim

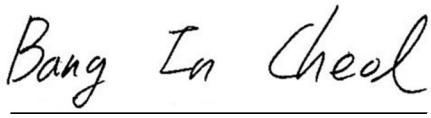

In Cheol Bang: Thesis Committee Member #1

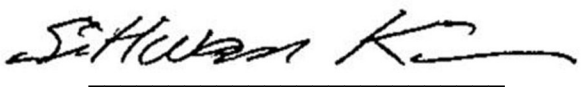

Si Hwan Kim: Thesis Committee Member #2

Abstract

Prediction of Fuel Cladding Performance for Ultra-long Cycle Fast Reactor Application

Ju Ang Jung

Nuclear Science and Engineering Program
The Graduate School
Ulsan National Institute of Science and Technology

As a part of R&D activities for the design of advanced fast reactors, the feasibility of ultra-long cycle fast reactors (UCFR) based on the assessment of key technical issues is investigated. The concept for UCFR is designed to be operating with no refueling during the overall operation period, so the design requirement for the fuel cladding such as creep rupture and swelling would be more challengeable than that in conventional fast reactors. The total operation period of UCFRs is varied from 30 to 60 years, the peak cladding temperature is 650℃ or higher, and the maximum neutron damage can go up to 300 dpa (displacement per atom) or higher depending on the specific core design.

In this study, several key design parameters for UCFR fuel claddings including the internal pressure cause by fission gas release, thermal creep, irradiation creep and swelling are technically evaluated on the basis of UCFR concepts proposed.

Considering the overall operation time of UCFR from 30 to 60 years, a large amount of fission gas is expected to be up inside of fuel cladding. This may raise a several technical issues on the safety of the cladding. There are various equations to formulate and model the fission gas release (FGR) in each type of nuclear metallic fuels.

The definition of irradiation creep is the difference in dimensional changes between a stressed and an unstressed samples irradiated under identical conditions. Also irradiation creep occurs when external non-hydrostatic stresses are applied during irradiation. And thermal creep is severe issue in materials that exposed to high temperature environment for long time. This study briefly summarizes especially with respect to their possible inter-correlation between irradiation creep and thermal creep. When high neutron dose by long operation time with no refueling (30years), high temperature and internal pressure (about 400dpa, 600℃ and 470MPa, respectively) applied to UCFR, either high irradiation creep or thermal creep can occur. Therefore this part should be thoroughly examined and evaluated.

Swelling is mainly caused by the increase of volume and decrease of density of materials subjected to intense neutron radiation. The operation environment of UCFR is high neutron dose (near 400dpa). It causes serious problem in cladding material because of swelling. After the threshold fluence of 10^{22}n/cm^2 is achieved, the swelling is exponentially increased. After the fluence threshold of 10^{22}n/cm^2 is attained, early experience characterized the increase of swelling in terms of an exponential rise.

The candidate cladding materials include ferritic-martensitic steels (FM steels), oxide dispersion strengthened steels (ODS steels), and SiC/SiC$_f$ composite. Among these materials, the result of this study shows that the SiC/SiC$_f$ composite is the most promising cladding material which would meet the fuel cladding design criteria for UCFR because of favorable material properties under high burnup and radiation environment.

Contents

I. Introduction

1.1 General Backgrounds

As a part of R&D activities for the development of advanced fast reactors, feasibility of the development of ultra-long cycle fast reactor (UCFR) based on the assessment of key technical issues is investigated. The concept for UCFR is designed to be operating without refueling during the total operation period, so the requirement for the fuel cladding such as creep rupture and swelling will be also more challenging. The total operation period of UCFRs is varied from 30 to 60 years, peak cladding temperature is 650℃ or higher, and the maximum neutron damage is 400dpa (displacement per atom) or higher depending on the specific design.

The concept of Ultra-long Cycle Fast Reactor (UCFR) was introduced in 1950s and recently it is being actively investigated as a mean to improve fuel utilization and solve the nuclear proliferation issues [1 – 5]. The benefits of UCFR include capital / operation cost reductions, low proliferation risk, and the interim storage of LWR spent fuel [1]. The CANDLE [2] design is one of thoroughly studied UCFRs. Its active core moves along the axial direction as the core burns and eventually the core reaches an equilibrium state. Natural uranium was used as blanket and liquid sodium and LBE (Lead Bismuth Eutectic) were used as coolant materials. Similarly to the CANDLE design, TerraPower Inc. has been developing a design of UCFR, TWR (Traveling Wave Reactor) [4]. Recently a modification has been introduced to TWR, adopting fuel assembly shuffling strategy rather than the axial movement of active core, which is called as SWR (Standing Wave Reactor).

Table 1.1 is comparing PWR, SFR and UCFR for fuel, refueling time, hoop stress, peak temperature and neutron damage. Fuel is U^{238} same as SFR. Hoop stress exceeds 400MPa and cladding temperature exceeds 600℃. Fluence is $2.94\times10^{24}n/cm^2$. The most important characteristic of UCFR is refueling time. Refueling time is ranged from 30 years to 60 years. So, it is the Ultra long Cycle Fast Reactor.

The Table 1.2 is for reactor environments comparing with other 4 SFRs.[4][6][7] All about temperature is similar to that of these 4 reactors. But the fluence is different. The fluence of UCFR is the largest in the all reactors. Because formula of fluence have a time parameter. The Table 1.3 is cladding design criteria for 4 reactors. Criteria elements are thermal strain, total strain, swelling, allowable temp and dpa. These elements are roughly similar between UCFR and other. Thermal strain is under 1%, total strain is under 3%, swelling is under 5% and cladding allowable temp is under 650℃. Neutron damage is same to fluence, so UCFR is particularly high comparing to others.

Goal of research and development, our main goal is selecting the candidate materials. Our second goal is to predict the life of candidate material. This study takes a theoretical approach to UCFR cladding materials. UCFR concept has too long cycle and too many neutrons so, we cannot do experiment for this study in university. Therefore I gathered and synthesized existing researches for finding the most suitable model for UCFR in this study.

In this thesis, several key design parameters for UCFR fuel cladding design including the internal pressure from fission gas release, irradiation creep and swelling are technically reviewed. In the later part of this thesis, life prediction based on creep rupture is also discussed.

1.2 The Goal and Scope of this Study

This chapter describes the goal of research and development. The one of the goal is establishment of UCFR fuel cladding and structural material database. Research and analysis related academic materials and technology report based on the results of a study is needed. Previous research should be collected about cladding materials and structural materials basic properties as high temperature tensile, fatigue, fracture toughness at design operating temperature.

The main goal of this study is preliminary life prediction of UCFR fuel cladding and structural material. The material of cladding theoretical life prediction is used with property data obtained. For each material conducted life preliminary assessment for feasibility in UCFR by Larson-Miller parameter and cladding design criteria. Selected cladding and structural material candidates for UCFR based on the results of life preliminary assessment.

Table 1.1 Comparing UCFR and other type reactors.

	PWR	**SFR**	**UCFR**
Fuel	U^{235} (0.71%)	U^{238} (99.29%)→Pu^{239}	**U^{238} (99.29%)→Pu^{239}**
Refueling time	18months	18months	**No refueling**
Hoop stress	40~80MPa	200MPa	**468MPa**
Peak temp.	320℃	650℃	**650℃**
Max. Neutron Damage	65dpa	200dpa	**N/A**
Max. Neutron Fluence	4.5×10^{22} n/cm^2	5.0×10^{23} n/cm^2	**2.94×10^{24} n/cm^2**

Table 1.2 Comparing UCFR and other reactors about reactor environment [4][6][7]

	KALIMER 600	JSFR	TWR_TP-1	UCFR
Fuel type / Cladding material	U-10Zr / HT9	MOX / PNC-ODS	U-10Zr / HT9	U-10Zr / HT9
Coolant	Sodium	Sodium	Sodium	Sodium
Core Power (MWe)	600	1500	1200	1000
Inlet Temperature (℃)	370	395	235	N/A
Outlet Temperature (℃)	545	550	523	N/A
Fuel Temperature (℃)	650	700	N/A	N/A
Max. Neutron Damage	200	250	350 (20% Burnup)	N/A
Max. Neutron Fluence (n/cm^2)	4.0×10^{23}	5.0×10^{23}	N/A	2.94×10^{24}
Refueling time (year/cycle)	1.5	2.2	40	60

Table 1.3 Comparing UCFR and other reactors about cladding design criteria [4][6][7]

	KALIMER 600	JSFR	TWR_TP-1	UCFR
Thermal strain (%)	**< 1**	**< 1**	**< 1**	**< 1**
Total strain (%)	**< 3**	**< 3**	**< 3**	**< 3**
Swelling (%)	**< 5**	**< 5**	**< 7**	**< 5**
Cladding allowable Temperature (℃)	**630**	**700**	**650**	**650**
Max. Neutron Damage	**200**	**250**	**350 (20% Burnup)**	**N/A**

II. Literature Study

The Literature study is for cladding candidate materials at UCFR. The materials are predicted there life at the later part of this chapter. The candidate materials include HT9 and T91 of ferritic martensitic steels, 12Y1 and 12YWT of oxide dispersion strengthened steels and SiC/SiC_f composite. These materials are studied at this chapter.

2.1 Introduction

- Fission Gas Release

The main contributors to fission gas release in metal fuel are xenon and krypton because of their virtually complete insolubility in the fuel matrix. Therefore, if kinetically favorable, xenon and krypton will be rejected from the fuel matrix. These gases are either directly released into the plenum, or accumulate in small bubbles within the fuel. Because the density of the gas in such bubbles is considerably lower than that of the solid fuel, gas atoms residing in bubbles occupy more volume than either the fissile atoms they replaced or fission-product atoms that segregate as solid phases. The precipitation of fission gases thus leads to swelling of the fuel to a larger degree than the volume expansion that would occur if the xenon and krypton had remained dissolved on an atomic scale in the fuel matrix. Swelling adversely affects fuel performance because it promotes fuel-cladding mechanical interaction, which may shorten the cladding lifetime.

- Internal Pressure

Fission gas is filled in the cladding. The cladding has high internal pressure as time passes because of fission gas.

- Thermal creep

Thermal creep, which becomes important for Zr alloys only above 300-350°C(depending on material and stress) and is affected by the irradiation induced microstructural changes. “Thermal creep” in-reactor is quite different from thermal creep of un-irradiated material. [8]

- Irradiation creep

Irradiation creep, which is only weakly depends on temperature and is the major contributor in the temperature range of interest for water-cooled reactors. The in-reactor creep depends primarily on stress, fast neutron flux, and temperature, but also on material conditions. [8]

- Swelling

Neutron-induced swelling is the increase of volume and decrease of density of materials subjected to intense neutron radiation. Neutrons impacting the material's lattice rearrange its atoms, causing buildup of dislocations, voids, and Wigner energy. Together with the resulting strength reduction and embrittlement, it is a major concern for materials for nuclear reactors.

2.2 Cladding Design Criteria

The cladding design criteria is the standard when cladding is designed.(Table 1.3) The cladding design criteria of KALIMER600(SFR) is thermal strain 1%, total strain 3%, swelling 5%, cladding allowable temperature 630℃ and neutron damage 200dpa. SFR's is similar to PWR's. The cladding design criteria of JSFR and TWR-TP1 are thermal strain 1%, total strain 3%, JSFR's swelling 5%, TWR's swelling 7%, cladding allowable temperature 650℃. The reason of cladding allowable temperature 650℃ is eutectic melting. [4][6][7]

2.3 Candidate Materials

2.3.1 Ferritic Martensitic Steels

2.3.1.1 HT9

The void swelling of HT9 was found in both alloys at 208dpa to occur at rates of 0.012%/dpa or less. The creep rate of HT9 is rather nonlinear in its response to hoop stress level in the range 0-200MPa, but 9Cr-1Mo exhibits only slightly greater than linear behavior with stress level. Irradiation of HT9 to very high neutron exposure at u 400°C confirms the inherent swelling resistance of this class of steels. The creep rate of HT9, however, exhibits a stress exponent of ~2 at this temperature. As normalized, 7–12%Cr steels contain a high number density of dislocations (Fig 2.10(a)). To increase toughness and ductility, normalized steel is tempered. During tempering, M23C6 (M is primarily Cr, Fe, and Mo) and MX (M is primarily vanadium and niobium, and X is carbon and nitrogen) precipitate (Fig 2.10(b)), resulting in a ferrite matrix with the large (60–200 nm) M23C6 particles on lath and prior-austenite grain boundaries and smaller (20–80 nm) MX particles in the matrix. In addition, the high number density of dislocations in the untempered martensite is reduced. Creep-rupture properties of T92 are a significant improvement over those for HT9, modified 9Cr–1Mo, and the reduced-activation steels (Fig 2.8). This strength advantage is evident when 105h rupture stresses are compared for the five steels at 550, 600, and 650℃ (Fig 2.9). [9]

2.3.1.2 T91

Void swelling of T91 was found in both alloys at 208dpa to occur at rates of 0.012%/dpa or less. Irradiation of 9Cr-1Mo to very high neutron exposure at u 400°C confirms the inherent swelling resistance of this class of steels. The irradiation creep rate of 9Cr-1Mo is roughly linear with stress and comparable to that of other ferritic steels. Swelling shows a strong dependence on irradiation dose (Fig 2.6(c)) in helium pre-implanted T91. The swelling in the 720appm He sample tripled when it was irradiated to 9.2dpa.[13][14] The microstructures of F82H and T91 steels prior to irradiation are quite similar. Both steels have a typical martensitic lath structure containing dislocations with a density of approximately $1\times10^{14}m^{-2}$. The dislocation density in T91 steel is slightly higher than in F82H. M23C6 type carbide precipitates were identified mainly along prior austenite grain boundaries and martensite lath boundaries. The size of precipitates varies from few tens nm to ~2μm, see Fig 2.13. After irradiation, the density and size of defect clusters in a T91 sample are almost the same as those in a F82H sample at the same dose. In both steels, the size increases while the density drops rapidly with irradiation temperature above about 250℃. The helium bubbles observed in T91 steel have slightly higher density and smaller size as compared to those in F82H steel irradiated at the same conditions. [15]

2.3.2 Oxide Dispersion Strengthened Steels

2.3.2.1 12Y1, 12YWT

12YWT contained a high density of extremely fine Y–Ti–O clusters, compared to the much larger oxide particles in the 12Y1. The fine dispersion of particles gave the 12YWT better tensile and creep properties compared to commercial ODS alloys and ferritic/martensitic steels that would be replaced by the new ODS steel. TEM microstructures of as-processed 12Y1 and 12YWT were considerably different (Fig 2.15). The 12YWT contained up to an order of magnitude more dislocations pinned by a fairly uniform distribution of very fine particles, whereas the 12Y1 contained much larger particles less uniformly distributed. The vanadium alloy creep curve is in the tertiary creep stage prior to rupture (the specimen failed after 4029 h and 52%), the 12YWT steel at 5000 h appears to be in the steady-state creep stage.[11] The strength of this steel decreases rapidly above 600℃, which is near the limit for such a steel. The superior strength of the 12YWT over the 12Y1 is obvious in this figure, and this is consistent with the difference expected based on the large difference in the microstructures. Indeed, because of the much larger and less evenly distributed oxide particles in the 12Y1.[11]

2.3.3 SiC/SiC_f composite

In Fig 2.19, scanning electron microscopic images are provided for fracture surfaces of the composites in non-irradiated and three different irradiation conditions. The fracture surfaces shown in the low magnification micrographs are rather brittle, showing that the interfacial frictional stresses in these composites are relatively high. While the typical fiber pull-out length was 5–10μm in the non-irradiation condition, it became slightly longer (5–20 lm) after irradiation at 570℃ – 2.2dpa or at 1000℃ – 5.3dpa. Contrarily, fracture surface of the composite irradiated at 350℃ – 1dpa appeared more brittle with the typical fiber pull-out length < 5μm. There was no noticeable effect of irradiation on fracture surface appearance of the SA3 composites, showing the typical fiber pull-out length 5–30 μm in all conditions. Neutron irradiation of bare fibers at higher temperatures apparently caused significant strength degradation. However, examination by scanning electron microscopy did not reveal the influence of irradiation on the surface appearance of the fibers, Fig 2.18.[16] Fig. 22 plots both historical data and published and unpublished data from a recent high-temperature irradiation study [218]. This plot is limited to literature data on high-purity CVD SiC. A divergence from point-defect ‘saturated’ swelling to non-saturated swelling is observed in the 1073–1473 K range, though additional data in this temperature range as a function of fluence would be required to precisely define such behavior. Above 1273 K, there exists a clear non-saturated swelling behavior for CVD SiC.[17] The potential for these materials have been widely discussed and is now understood to be (1) the ability to operate in temperature regimes much higher than for metallic alloys, (2) an inherent low level of long-lived radioisotopes that reduces the radiological burden of the structure, and (3) perceived tolerance against neutron irradiation up to high temperatures. Advanced (Generation III) SiC fiber, CVI SiC matrix composites have been evaluated as the current reference materials. Various interphase configurations and reinforcement architectures have been studied for improved radiation stability, strength, and thermal conductivity. Advanced characterization tests, including fiber/matrix interfacial friction and time-dependent deformation, have been developed. Baseline property characterization and low dose irradiation studies were completed for PG3 NITE SiC/SiC_f as a promising alternate material.[18]

2.4 Life Prediction Model

2.4.1 Fission Gas Release

Fission gases are considered to be released from the fuel when they reach any space that is connected to the free volume within the fuel pin. Gas connection zones include the fuel/cladding gap and the porosity within the fuel which communicates directly with the gap (open porosity). The following is assumed regarding the gas in the closed bubbles and that in the free volumes (plenum above the fuel slug and open porosity within the fuel slug):

1. Once the gas is released into the free volumes, its probability of reentering the closed bubbles is zero.

2. The gas pressure in open porosity is equal to that in the plenum. Because of the insolubility of xenon and krypton in solids, there is no direct influence of plenum pressure on the rate of gas escape from the fuel.

3. While the fission gas within the closed bubbles tends to cause swelling, the fission gas in the free volume promotes shrinkage by pressurizing the solid and thereby encouraging collapse of the internal porosity.

Considering the total operation period of UCFR which is 30 to 60 years, a large amount of fission gas is expected to be built up inside of fuel cladding. This may raise a several technical issues on the safety of the cladding. There are various equations to formulate and model the fission gas release (FGR) in various type of nuclear metallic fuels.

- M.C. Billone et al - Life-Metal code [20]

Empirical model, which calculates the fission gas release by a simple function using burnup, porosity and temperature. It does not explicitly consider the fission gas bubbles. It is inadaptable because fission gas bubble is not accurately considered.

- Y. Tsuboi et al - OGRES model [22]

The OGRES model, which was originally developed for oxide fuels, was modified for metallic fuel and adopted for the intragranular gas behavior. The OGRES model is partly different, but quite similar to the GRSIS model. The GRSIS model is a mechanistic model of fission gas release and swelling for the U-Pu-10Zr metallic fuel in a fast reactor, GRSIS (Gas Release and Swelling in ISotropic fuel matrix), was developed.

Intragranular gas model is as follows,

$$\frac{\partial C_t}{\partial t} = \frac{\partial}{\partial r}\left(\left(D_1 + D_2\right) r^2 \frac{\partial C_t}{\partial t} \right) + K_g,$$
$$D_1 = D_g (b-k) / (D_g K_b^2 + b),$$
$$D_2 = D_{gb} (D_{gb} - k) / (D_g K_b^2 + b). \tag{2.1}$$

where C_t : the concentration of total gas, K_g : the generation rate of gas atoms, D_g : the diffution constant of single gas atoms, D_{gb} : the diffusion constant of gas bubbles, b : the resolution coefficient, k : the bubble generation coefficient, r_b : the radius of the bubble

Grain boundary model is as follows,

The grain boundary model [4] assumes that coalescence and growth of bubbles by random and biased migration occur in grain boundaries.

Grain boundary bubbles are treated as follows:

(a) grain boundary bubbles are classified into six classes by the amount of gas atoms stored in bubbles;

(b) the number density of each bubble class is determined by the result of coalescence and bubble growth calculation;

(c) only class 6 bubbles represent open bubbles;

(d) bubble re-solution is neglected.

The equations describing coalescence and growth of the bubbles are written as

$$\frac{dC_i^l}{dt} = G_i^l + \sum_{j=1}^{i-1} R_{i-1\,j}^{'l} - \sum_{j=i}^{6} R_{ji}^l + E_i^l$$

for i=1 to 5

$$\frac{dC_6^l}{dt} = \sum_{i=1}^{5} R_{5i}^{'l}, \text{ for i=6} \qquad (2.2)$$

where superscript *l* means *l* th radial mesh, subscript i and j mean class i, j bubbles. G_i^l is the grain boundary bubble generation rate. It is assumed that intragranular atoms and bubbles which reached grain boundaries generate class *l* grain boundary bubbles. G_i^l (i > 1) is neglected presently. R_{ij}^l is the collision rate of class i with class j bubble and $R_{ij}^{'l}$ is the shifting rate from class i to class i + 1 due to coalescence of class i with class j. Therefore the second term of the right-hand side of upper equation is the growing up from class i - 1 to class i. The third term is the growing up from class i to class i + 1 absorbing lesser class bubbles. The fourth term represents the absorption of class i into the upper class.

Swelling model is as follows,

$$dv/v = \sum_{i=0}^{5} \left(m_i R T^l C_i \right) / P_{gi} + V_6$$

$$P_{gi} = 2\tau / r_i + P_c \qquad (2.3)$$

where V_6 is the volume of class 6 bubble (open bubble)(m^3), P_{gi} the fission product gas internal

pressure (Pa), τ the surface tension of fuel (N/m), r_i the bubble radius (m) and P_c the external pressure (Pa).

Gas release model is as follows,

Fission gas is modeled to be released only through class 6 bubbles which are assumed to be opened to the fuel surface, while bubbles in the other 5 classes are modeled to be closed bubbles. The class 6 bubble is formed by coalescence between the class 5 bubbles and bubbles from class 1 to 5. As the transformation from a closed bubble to an open one is considered to have relation to swelling, its probability is given as a function of local swelling (du/u) determined by eq. (13). In this model the probability f_{5j} is given as follows

$$f_{5j} = \begin{cases} 0 & \text{dv/v} < 0.05 \\ \left(dv/v - 0.05\right)/\left(0.1 - 0.05\right) & 0.05 < \text{dv/v} < 0.1 \\ 1 & \text{dv/v} > 0.1 \end{cases} \tag{2.4}$$

In this model, coalescences between class 6 and other less classified bubbles do not increase the class 6 bubble number density. In other words, fission gas contained in closed bubbles is directly released through class 6 bubbles to fuel surface without increasing their volume. Additionally open bubble swelling (class 6 bubble volume) is assumed to be saturated when the tunnels of open bubbles are fully developed. In order to model this saturation, an upper limit of swelling of open bubble, Bu, is introduced in class 6. After class 6 volume attains Bu, the volume does not increase any more by growing up of class 5 bubble to class 6.

Conclusion of OGRES model is as follows,

A mechanistic model of fission gas behavior in metallic fuel has been developed. The model covers swelling and fission gas release. Experimental data of irradiated uranium metal are analyzed by this model. For uranium metal, the result of this analysis shows that this model is valid to prediction fission gas swelling under steady-state and transient conditions. This model is considered to be applicable for homogeneous conditions such as y phase at high temperature. However additional models are necessary, e.g., for a phase and intermediate phase for U-Pu-Zr alloy. This model will be incorporated into a new mechanistic fuel pin performance code.

- T. Ogata et al - ALFUS model [19]

The models included in the ALFUS are thought reasonable and consistent with knowledge obtained from the irradiation test results. The ALFUS model which is based on UO2 fuel about bubble formation and growth is not suitable for metallic fuel.

In this model the following assumptions are made.

(a) FP gas atoms and gas bubbles in the grain migrate and form bubbles at the grain boundary, or are absorbed by the existing grain boundary bubbles. Equilibrium state in the grain is assumed among gas atom generation by the fission, the in-grain bubble formation, re-solution to the alloy matrix,

absorption by the in-grain bubbles. Both of the in-grain and the grain boundary bubbles are assumed to be spherical. Internal pressure of the bubbles equilibrates to the external hydrostatic force and the surface tension.

(b) The grain boundary bubbles coalesce with each other by collision due to their random migration. They also absorb the gas atoms and the in-grain bubbles. These two processes increase the size of the grain boundary bubble.

(c) When the volume fraction of the grain boundary bubbles increases over a threshold value, they begin interconnecting and form the open pore. The FP gas which has been included in the open pore is immediately released to the gas plenum.

(d) FP gas atoms and gas bubbles may collide with the open pore. It leads to gas release and increase in an open pore size.

(e) The gas bubbles and the open pore contribute to total swelling.

- W. Hwang et al – MACSIS code [23]

The fission gas release model of MACSIS code consists of intra-granular and intergranular fission gas release model.

The model of intra-granular fission gas release is as follows,

$$\frac{\partial c}{\partial t} = D\nabla^2 C + \beta$$
$$\text{subject to c = 0 at r = a, 0} \le \text{t:}$$
$$0 \le r \le a,\ \text{t} = 0 \tag{2.5}$$

The model of intergranular fission gas release is as follows,

$$\int_{n_i}^{n_{i+1}} F(m,\tau,n)dn = \bar{f}_i\left(n_{i+1} - n_i\right)$$
$$or:$$
$$\bar{f}_i\left(n_{i+1} - n_i\right) = 0.23m\cdot\tau^{-4/5}\int_{n_i}^{n_{i+1}}\left\{\exp\left(-A\left(n\tau^{-2/5} - 0.5\right)\right)\right\} \times\left\{\sin\ \mathrm{h}\left[B\left(n\tau^{-2/5} - 0.5\right)\right]^{1/2}\right\}dn \tag{2.6}$$

where

n_i = number of gas atoms in the i size bubble

τ = reduced time as a dimensionless parameter

$m' = m_{gb} / E_t$, the number of gas atoms per unit volume around the grain boundary surface

m_{gb} = number of gas atoms per unit area on the grain boundary

E_t = the effective thickness of grain boundary

A, B = dimensionless constants

– C.B. Lee et al - GRSIS code [20]

Among them, GRSIS (Gas Release and Swelling in Isotropic fuel matrix) model [1] has been thoroughly assessed based on the detail high burn-up irradiation experiments. For this reason, GRSIS code is used for the analysis of FGR of metallic fuel in UCFR in this study. The formulation of FGR is given as follows:

$\frac{dC_{gb4}}{dt}$ =gas diffusion into bubble-4 + integration of bubbles-1, 2 and 3 into bubble-4 by diffusion and growth + instantaneous increase by bubble interconnection at threshold closed bubble swelling,

where C_g is the gas atom concentration in the matrix .atoms=m3. and C_{gbi} is the gas atom concentration as the bubble-i in the matrix (atoms=m^3)

$\frac{dC_{gb4}}{dt}$ = J_{g4} + ab_{14} + ab_{24} + aab_{34} + gab_{14} + gab_{24}+ gab_{34} + instantaneous increase by bubble interconnection at threshold closed bubble swelling,

where Y is the fission yield of gas atoms (atoms/fission), F is the fission density (fission=s m3), J_{gi} is the gas diffusion to bubble-i (atoms=s m3), J_{b1nucl} is the bubble-1 nucleation rate (atoms=s m3), ab_{ij} is the integration rate of bubble-i into bubble-j by bubble diffusion (atoms=s m3), gab_{ij} is the integration rate of bubble-I into bubble-j by radial growth of bubble-i due to gas diffusion to bubble-i (atoms=s m3) and $f_{i, i+1}$ is the transition probability of bubble-i into bubble-i+1 by collision with bubble-i.

The relation of bubble density, N_{bi} and total gas atom density of bubble-i, C_{gbi} is

$$C_{gb_i} = atnb_i \cdot N_{b_i} \tag{2.7}$$

where $atnb_i$ is the density of gas atom in a bubble-i (atoms/bub-i) and N_{bi} is the bubble-i concentration (bub-i/m^3).

$$
\begin{aligned}
FGR &= 0,\ S_t < S_{th} \\
&= f_{th}(C_{gb1}+C_{gb2}+C_{gb3}),\ S_t = S_{th} \\
&= C_{gb4},\ S_t < S_{th}
\end{aligned}
\tag{2.8}
$$

where St = total swelling, S_{th} = threshold swelling, f_{th} = fraction of closed bubbles to be open at the threshold closed bubble swelling, C_{gbi} = gas atom concentration as the bubble-i in the matrix (atoms/m3)

Bubbles are classified in terms of radius, surface area, volume and atomic density. Bubble sizes should be selected from the microstructure analysis of the irradiated fuels. Threshold swelling and fraction of interconnected bubbles at the threshold swelling need to be set. The next step is reading of the irradiation history, such as time, fission rate and temperature. From the irradiation condition of the fuel, rate constants of the fission gas and bubble movements are calculated. Then, concentrations of gas atoms and bubbles are calculated. Bubble swelling is calculated from the bubble concentrations and threshold swelling for bubble interconnection to be open to the external open space is checked. Then, the fuel gap closure by fuel swelling is checked. When the fuel swelling becomes larger than the fuel gap allowance, bubble swelling is recalculated after increasing the contact pressure between fuel and cladding. As the contact pressure increases, fuel swelling by bubbles decreases. Therefore, it is iterated until fuel swelling is equal to the fuel gap allowance and then, the contact pressure is determined.

Input variables in the GRSIS model are fuel design parameters, a set of bubble characterizations, threshold bubble swelling and a fraction of interconnected bubbles and irradiation histories such as time, fission density and temperature. Then, the output of the GRSIS model is gas atom concentrations in the matrix, concentrations of bubbles, swelling by closed and open bubbles, fission gas release and contact pressure between fuel and cladding.

- T. Ogata et al – FEAST METAL model [21]

Figure-3 shows the fractional fission gas release as a function of burnup for the ANL U-Pu-10Zr irradiation database [26]. Fission gases at the fuel rod of peak power start to be released through open channels formed by interconnection of the bubbles at a burnup of about 0.5 %. Then, the fractional fission gas release increases to about 70 % when the burnup reaches 4-5 at % burnup and levels off at about 80 % at 10 at % burnup.

Many models have been developed for fission gas release and swelling behavior of the U-Pu-10Zr metallic fuel for liquid metal fast reactors. The model in the LIFE-METAL [18] code is empirical, and calculates the fission gas release by a simple correlation using burnup, porosity and temperature. It does not explicitly consider fission gas bubbles. The ALFUS [19] model considers the bubble formation and growth based upon a model originally developed for UO_2 fuel. Therefore, it is assumed that fission gases are generated inside the fuel grains and then diffuse to the grain boundaries to nucleate a new bubble or be absorbed by an existing bubble at the grain boundaries. However, in metal fuel the fission gas bubbles could nuc1eate at the phase boundaries inside grains as well as at the grain boundaries. The phase boundaries are distributed quite randomly inside the grains in U-Pu-1 0Zr metallic fuel. Therefore, the effect of grain size on fission gas behavior in metallic fuel may not be as important as in UO_2 fuel.

The FEAST-METAL user can select either a mechanistic fission gas release model or an empirical

one.

Mechanistic Model is as follows,

The GRSIS model [26] is adopted to model the fission gas behavior of the metallic fuel in the FEAST-METAL code. A schematic diagram of the fission gas bubble nucleation and growth in the metallic fuel according to the GRSIS approach is shown in Figure-4. Fission gas atoms are generated by fission, and then form (nucleate) new bubbles or diffuse into existing bubbles. The bubbles are assumed to nucleate uniformly from the gas atoms in the metallic fuel matrix, since they nucleate at both the grain boundaries and the phase boundaries which are randomly distributed inside grain. The closed bubbles can grow by the diffusion of newly created fission gas atoms, and are classified into two groups depending on their sizes. Small bubbles and large bubbles are defined as having 0.5 and 10 micron radius, respectively. The third group of bubbles is the open bubbles (or open pores), which are connected to each other and open to the external free space. They are assumed to be of the same type as the closed bubbles. When a closed bubble-i becomes an open bubble, it is assumed to be transformed into bubble-3i. When the fuel matrix swelling due to the closed bubbles reaches a threshold value, it is assumed that a certain fraction of the bubbles become interconnected and release their gas into the free volume (i.e., they become open bubbles).

According to the bubble classification given in Figure-4, the behavior of the fission gas atoms and bubbles can be described as follows. Bubbles in group 1 are nucleated from the fuel matrix. They can collide with each other by both diffusion and growth, to become bubbles in group 2, with the probability of this process depending on the difference of the bubble sizes between groups 1 and 2. When bubbles in group 1 or 2 collide with bubbles in group 3, they become part of group 3. Bubbles in group 3 (open bubbles) are designated as bubbles-31 and 32, depending on the bubble group from which it came. Open bubbles are assumed not to move (diffuse) since gases in the open bubbles are released into the free volume.

Empirical Model is as follows,

The upper part of the fission gas release data band given in Figure-3 represents the typical peak fuel pin fission gas release behavior of EBR-II reactor. πle data has been fitted to an exponential function as given in Eq-2.2.1 and shown in Figure-5.

$$f = \begin{cases} 0 & \text{Bu} \le 0.8 \\ 0.8 \times \left[1 - \exp\left(-\frac{Bu}{1.8} \right) \right] & \text{Bu} \ge 0.8 \end{cases} \qquad (2.9)$$

f: Fission gas release fraction, Bu: Average fuel rod burnup (at %)

This type of a relation is recommended for use only in rough comparative analyses. Because the metal fuel fission gas release behavior shows strong dependency on axial power profile, operating temperature and linear heat rate, such a simplified relation should not be used for studies, in which accuracy is required.

Finally note that the empirical treatment has been developed only for fission gas release, whereas the swelling behavior of the fuel is simulated with the GRSIS model, even when the fission gas release empirical correlation is selected.

2.4.2 Internal Pressure

The internal pressure equation is from the ideal gas equation, derived as follows $\frac{P_p V_p}{T_p} = \frac{P_0 V_0}{T_0}$ (2.10)

where P_p = Plenum pressure when the end of fuel rod, α_0 = The volume of fission gas release per cubic at standard temperature and pressure(273K, 1atm), V_o=initial volume=The volume of fission gas release at standard temperature and pressure, V_f=active fuel volume.

$V_o = \alpha_0 V_f$ (2.11)

(2.10)+ (2.11) = $\frac{P_p V_p}{T_p} = \frac{\alpha_0 V_f P_0}{273}$ (2.12)

$\frac{V_p}{V_f} = \frac{L_p}{L_f}$ (2.13)

(2.12)+ (2.13) = $P_p = \alpha_0 L_f \frac{T_p P_0}{273 L_p}$ (2.14) → $P_p L_p = \alpha_0 L_f \frac{T_p P_0}{273}$ (2.16)

$\alpha_0 = \frac{FnRT_0}{P_0}$ (2.15)

where F=fission gas release fraction, R=universal gas constant (8317 J/kg·mol·K), n=kg·mol fission gas produced/m3 fuel. [24]

2.4.3. Thermal Creep

- R. J. Amodeo et al [25]

The correlation by Amodeo and Ghoniem employs the minimum commitment method (MCM) and uses time dependent creep strain curves at 873 K, as reported by Sandvik Steels. The MCM is based on the observation that the 1% strain occurs during either the primary creep regime or at the beginning of the secondary creep regime, and that the 5% strain occurs at the boundary between the secondary and tertiary creep regimes.

- G. Lewis and C. C. Chuang [26]

The correlation proposed by Lewis and Chuang uses the theta projection method (TPM). The TPM method is a numerical method employing the following equations. For long-life applications, the TPM model is known to have advantages over other models because its equations are more suitable for long-life extrapolation.

- H. J. Ryu et al [27]

Both the above two methods did not match exactly, so creep developed a new model is calculated by dividing the three regimes. Creep correlation for primary and steady-state regimes by using the Garofalo equation. Creep model for tertiary creep regime by using the Monkman–Grant relationship.

$$\varepsilon_{ps} = \varepsilon_p \left[1 - \exp\left(-mt\right)\right] + \dot{\varepsilon}_s t$$

where

$$P_o(T) = 0.52 - \frac{2647.31}{T}$$

$$P_1(T) = 1.09 - \frac{31.48}{T} \qquad (2.17)$$

$$\log \varepsilon_p(\%) = P_0(T) + P_1(T) \log \sigma_{eff}(MPa)$$

We also obtained the following steady-state creep strain rate in the higher stress exponent regime (n=19.7) as follows:

$$\log \dot{\varepsilon}_s \left(S^{-1}\right) = S_h(T) + 19.7 \log \sigma_{eff}(MPa)$$

$$S_h(T) = -13.84 - \frac{32657.11}{T} \qquad (2.18)$$

$$t_r \dot{\varepsilon}_s^q = C$$

$$\lambda = \varepsilon_r / \varepsilon_s = \dot{\varepsilon}_{ave} / \dot{\varepsilon}_s$$

$$\varepsilon / \varepsilon_r = 1 - (1 - t / t_r)^{1/\lambda} \qquad (2.19)$$

$$\log \sigma_r = R_0(T) + R_1(T) \log t_r$$
$$R_0(T) = 32.65 - \frac{49039}{T} + \frac{20048000}{T^2},\ R_1(T) = -12.97 + \frac{20373}{T} - \frac{8041900}{T^2} \tag{2.20}$$

2.4.4. Irradiation Creep

The definition of irradiation creep is the difference in dimensional changes between a stressed and an unstressed sample irradiated under identical conditions. Also irradiation creep occurs when external non hydrostatic stresses are applied during irradiation. And thermal creep is severe in materials that are subjected to heat for long periods, and near melting point. This thesis briefly summarizes especially with respect to their possible inter-correlation between irradiation creep and thermal creep. When applied to UCFR, high neutron dose by long refueling time, 30 years, and high temperature and pressure (near 400dpa, 600℃, 470MPa) can produce high irradiation creep as well as thermal creep. Therefore this part should be thoroughly examined and tested. The equation regarding irradiation creep strain is expressed as follows,

$$\varepsilon_{irr} = B\sigma^{n}{}_{e}\phi t + DS_0\sigma_e \tag{2.21}$$

where ε_{irr} = irradiation effective creep strain, Φt = fast neutron fluence (10^{22} n/cm^2), σ_e = effective stress (MPa), n = stress exponent(1.3), B = irradiation creep coefficient(-2.9+9.5x10^{-3}T(10^{-26}MPa-1.3cm^2/n)), D = swelling enhanced creep coefficient(6.1(10^{-6}MPa^{-1})), S_0 = initial swelling(%)

- A.Boltax et al [28]

The effect of the swelling stress of annealed and cold-processed 316SS. Annealed material shows that the more sensitive to stress.

$$\varepsilon_{irr}(\%) = C\sigma_e^{n}\phi t + DS_0\sigma_e,\quad \frac{\varepsilon}{\sigma} = C\phi t + DS \tag{2.22}$$

where S_0 = stress free swelling, S = total swelling, σ=effective stress, ε=effective creep strain, φt = fast fluence, C and D material coefficients, D=2*10^{-7}

- M. B. Toloczko et al [29]

The creep rate is considered under the influence of creep compliance even if there is no swelling.

$$\overline{B} = \frac{\dot{\overline{\varepsilon}}}{\overline{\sigma}} = B_0 + D\dot{S} \tag{2.23}$$

where $\overline{B}$ = stress normalized effective creep rate, B0=creep compliance, D=creep-swelling coupling coefficient, $\dot{S}$ =volumetric swelling rate

– J. E. FLINN et al [30]

The creep experiments use the annealed 304SS at EBR2 reactor. The effect of stress about swelling and irradiation creep is shown as follows,

$$\dot{\bar{\varepsilon}} = (B\phi + D\dot{S}_0)\bar{\sigma} \tag{2.24}$$

where $\dot{\bar{\varepsilon}}$ = effective strain rate, h-1, Φ= neutron flux (E > 0.1 MeV), $\dot{S}_0$ = swelling rate with no applied stress, h^{-1}, $\bar{\sigma}$ = effective stress, psi, B= coefficient to describe creep in the absence of swelling, $(n/cm^2\ see)^{-1}$, D= coefficient for effect of swelling on creep, psi^{-1}

2.4.5.Swelling

Swelling is mainly caused by the increase of volume and decrease of density of materials subjected to intense neutron radiation. The operation environment of UCFR is high neutron dose (near 400dpa). It causes too serious problem in cladding material because of swelling. After the fluence threshold of $10^{22}n/cm^2$ is attained, early experience characterized the increase in terms of an exponential rise [6]:

$$\left(\frac{\Delta V}{V}\right)_{swelling} \propto [\phi t]^n \tag{2.25}$$

where n is greater than unity.

A form of the stress-free void swelling relationship that has received widespread usage is as follows:

$$\left(\frac{\Delta V}{V}\right) = \frac{V_f - V_0}{V_0} \cong (0.01)R\left[\phi t + \frac{1}{\alpha}\ln\left(\frac{1+\exp\left[\alpha(\tau-\phi t)\right]}{1+\exp(\alpha\tau)}\right)\right] \tag{2.26}$$

where V_f = final specimen volume, V_0 = initial specimen volume, R = swelling rate parameter in units of % per 10^{22} n/cm^2 (E>0.1MeV), Φt = neutron fluence in units of 10^{22} n/cm^2 (E>0.1MeV), α = curvature parameter in units of $(10^{22}n/cm^2)^{-1}$, τ = incubation parameter in units of 10^{22} n/cm^2 (E>0.1MeV)

– J. E. FLINN et al [30]

The creep experiments use the annealed 304SS at EBR2 reactor. The effect of stress about swelling and irradiation creep is shown as follows,

$$\dot{S} = \dot{S}_0 \left(1 + P\sigma_H\right)$$
$$\sigma H = (\sigma 1 + \sigma 2 + \sigma 3)/3$$
$$\dot{\varepsilon}_{total} = \frac{3}{4} B\phi\sigma + \frac{1}{3}\dot{S}_0 + (D + \frac{2}{9}P)\frac{3}{4}\dot{S}_0\sigma \quad (2.27)$$

where $\dot{S}_0$ = swelling rate with no applied stress, h^{-1}, P=coefficient for effect of stress on swelling, psi^{-1}, σ_H=hydrostatic stress, psi

- J. P. FOSTER et al [31]

Measuring residual stress at tube by 304SS. The biggest cause of residual stress is stress between swelling and irradiation creep.

$$\dot{S} = \dot{S}_0 \left(1 + P\sigma_H\right) \quad (2.28)$$

where $\dot{S}_0$ =swelling rate, P=assumed to be temperature independent across the tube wall thickness, though not necessarily independent of fluence.

- A. Boltax et al [32]

The performance experiment of MOX, Mixed carbide fuel and the trend for the study about Carbide fuel. They calculate the fuel performance using by Cygro-F computer code.

$$\dot{S} = \dot{S}_0 \left(1 + P\sigma_H\right) \quad (2.28)$$

where $\dot{S}$=total swelling, $\dot{S}_0$ =stress free swelling, P=material constant, σ_H= =hydrostatic stress

Table 2.1 Data used in calculation

Re-solution coefficient, b	10^{-6} l/s
Bubble generation coefficient, k	10^{-7} l/s
Gas atom diffusion coefficient, D_g	$D_g=1.4\times10^{-5}\exp(-5200/RT)m^2/s$ [a)]
Surface diffusion coefficient, D_s	$D_s=16.6\exp(-40T_m/RT)+1.4\times10^{-6}\exp(-13T_m/RT)m^2/s$ [a,b)]
Grain size	10 μm
Surface tension (γ phase uranium)	0.8 N/m
Critical swelling (tunnel volume)	0.07
[a)] R is the gas constant (1.98) and T the temperature (K).	
[b)] T_m is the melting temperature of the uranium metal.	

Table 2.2 Chemical composition of HT9 [10]

	C	Cr	Mo	Ni	Mn	V
HT9	n.i.	11.8	0.99	0.48	0.5	0.29

Table 2.3 Chemical composition of T91 [10]

	C	Cr	Mo	Ni	Mn	V	Nb
T91	n.i.	9	1	0.09	0.42	0.3	0.3

Table 2.4 Chemical composition of 12Y1, 12YWT [11]

	Cr	W	Ti	Y_2O_3
12Y1	12	0	0	0.25
12YWT	12	2.5	0.4	0.25

Table 2.5 Calculated creep coefficients [13]

Alloy	B_0, $\times 10^{-6}$MPa^{-1}dpa^{-1}	D, $\times 10^{-2}$MPa^{-1}
FFTF HT9	0.95	0.59
PFR HT9	1.7-1.9	a
D57	0.4-0.5	a
MA957	0.25-0.60	a

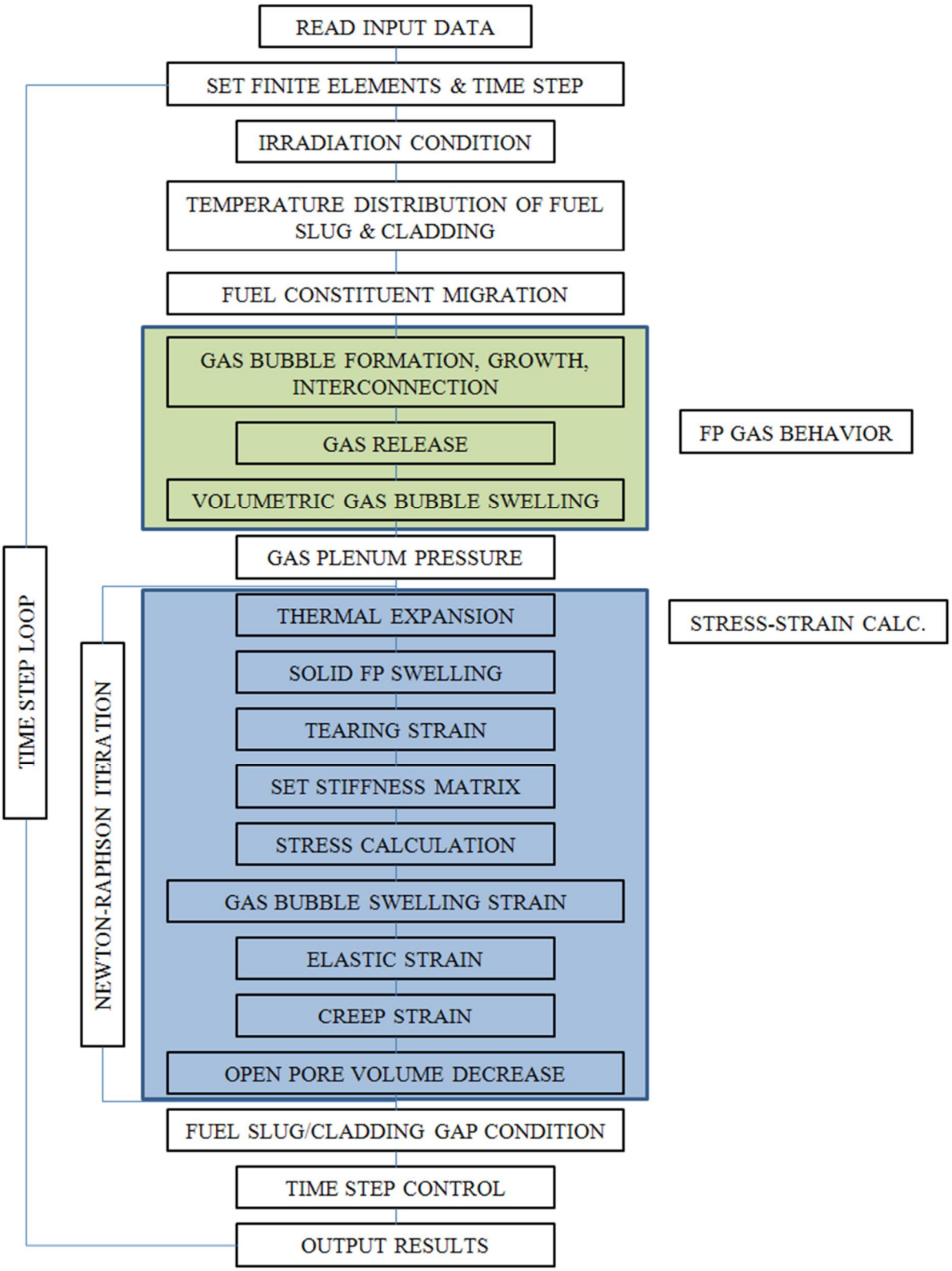

Fig 2.1 Calculation flow of the ALFUS code [19]

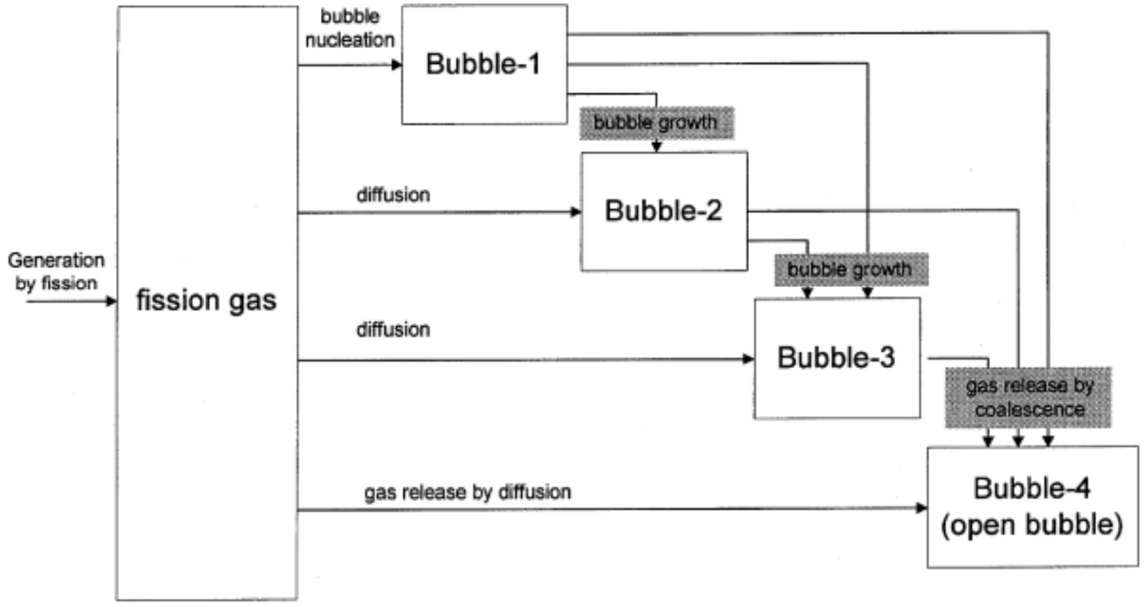

Fig 2.2 Fission gas and bubble movement in the GRSIS model [20]

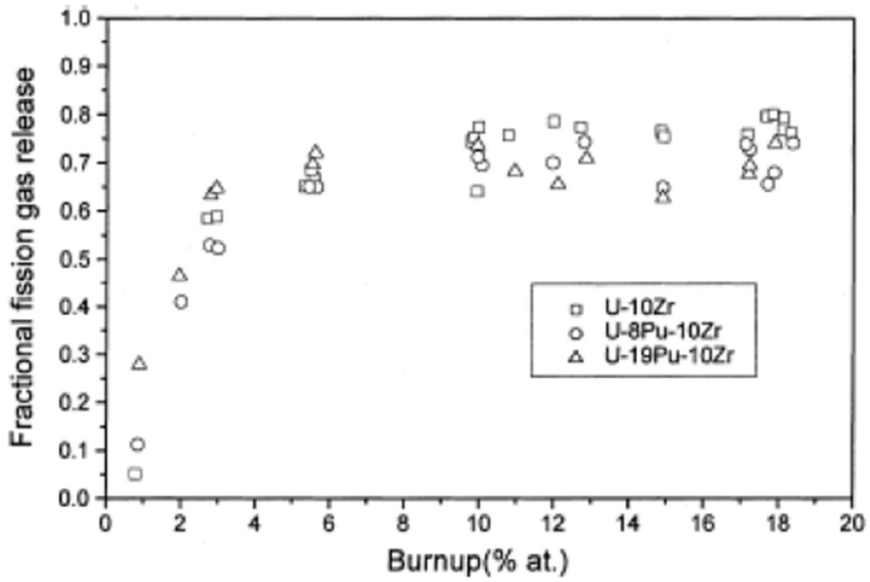

Fig 2.3 Fission gas release of ANL fuel irradiation tests [20]

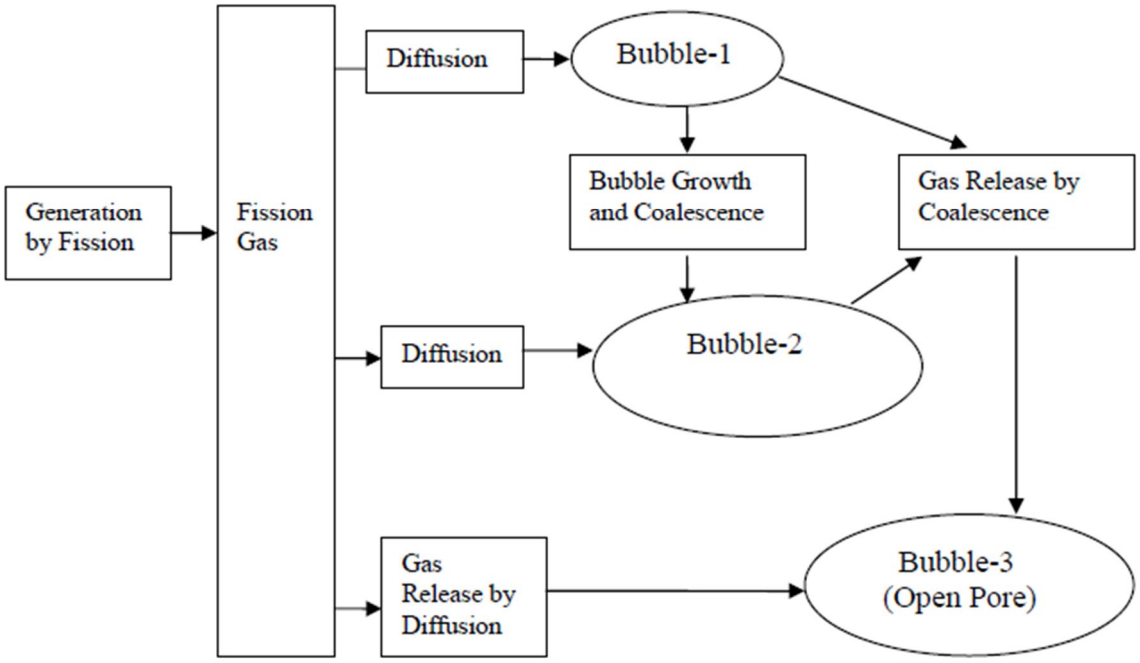

Fig 2.4 Fission gas and bubble movement model [21]

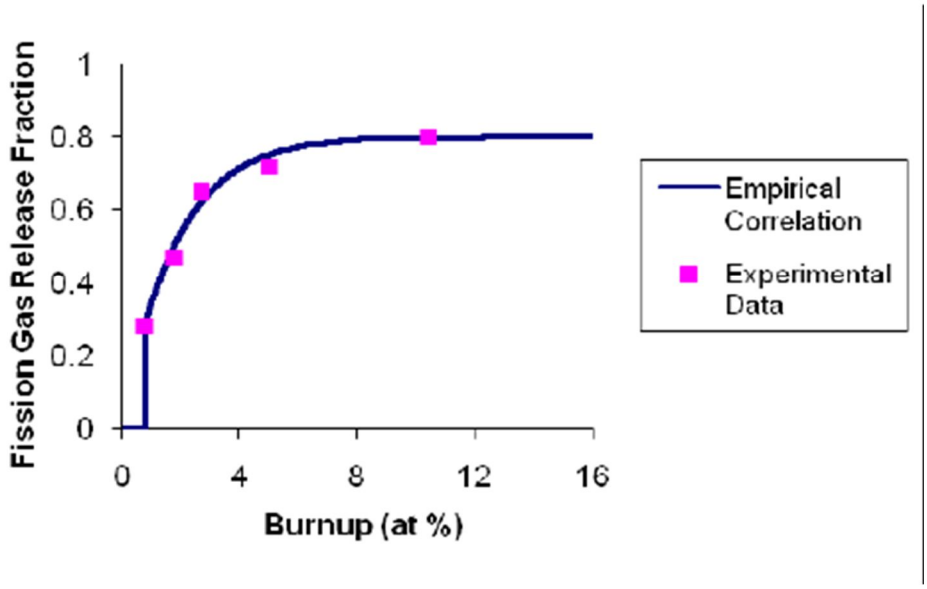

Fig 2.5 Empirical correlation for fission gas release (experimental data) [21]

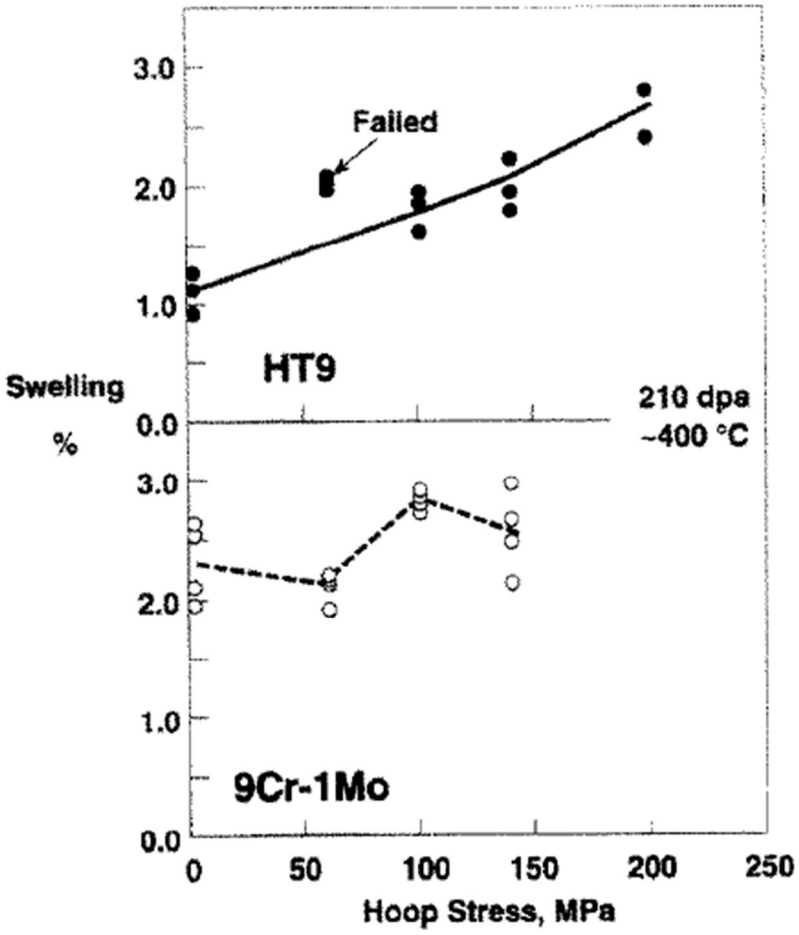

Fig 2.6 Swelling measured for individual tube segments at 208dpa [13]

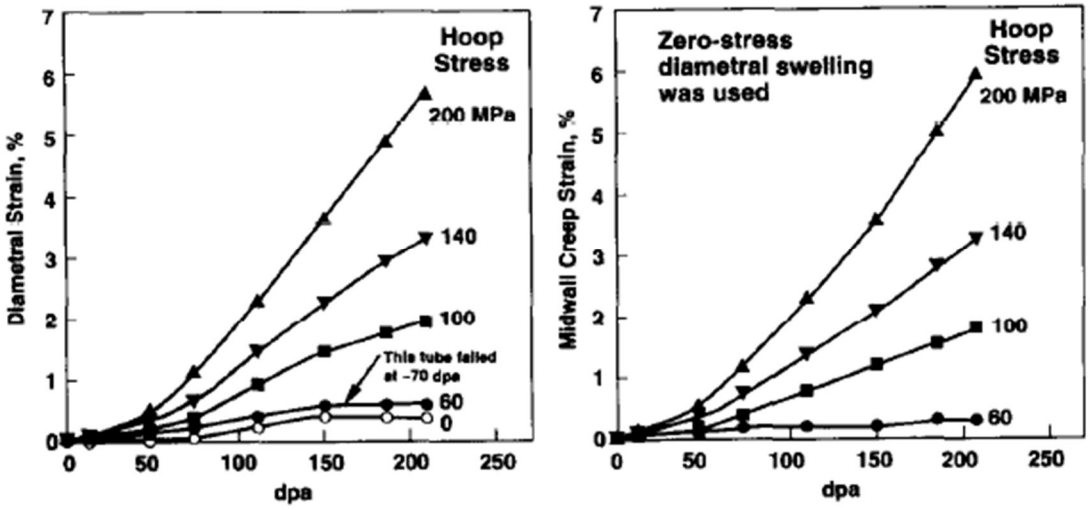

Fig 2.7 Total diametral strains and midwall creep strains for HT9 [13]

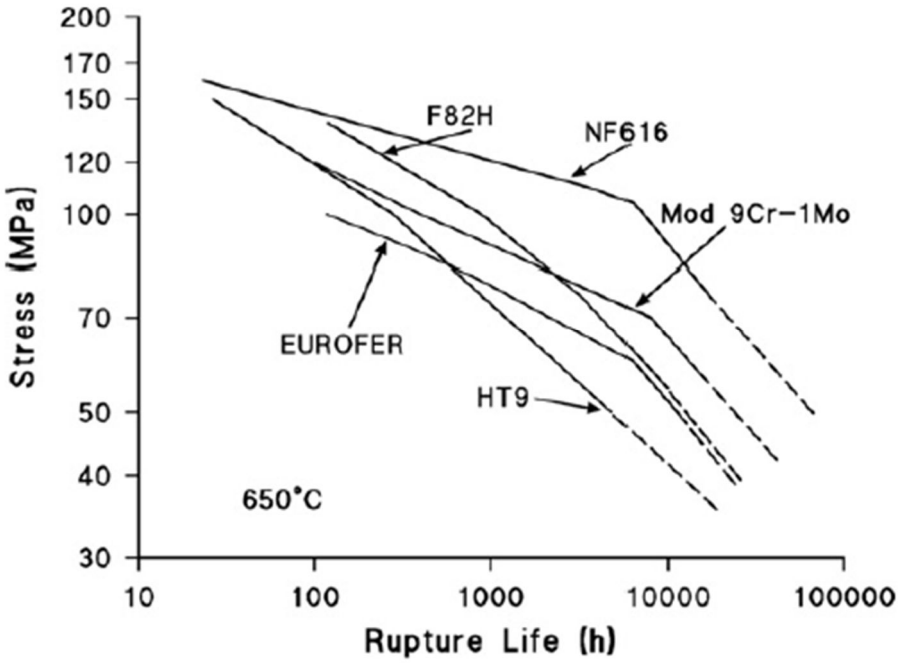

Fig 2.8 Comparison of the creep-rupture curves for tests at 650℃ for commercial steels Sandvik HT9, modified 9Cr-1Mo, NF616, F82H, and EUROFER [9]

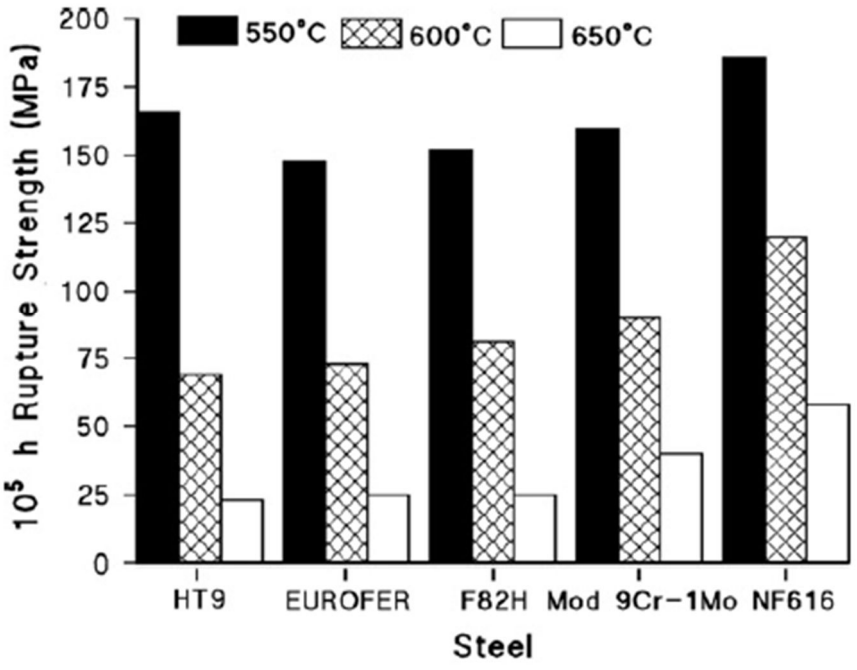

Fig 2.9 A comparison of the 100000h rupture strengths for Sandvik HT9, EUROFER, F82H, modified 9Cr-1Mo, and NF616 at 550, 600, and 650℃ [9]

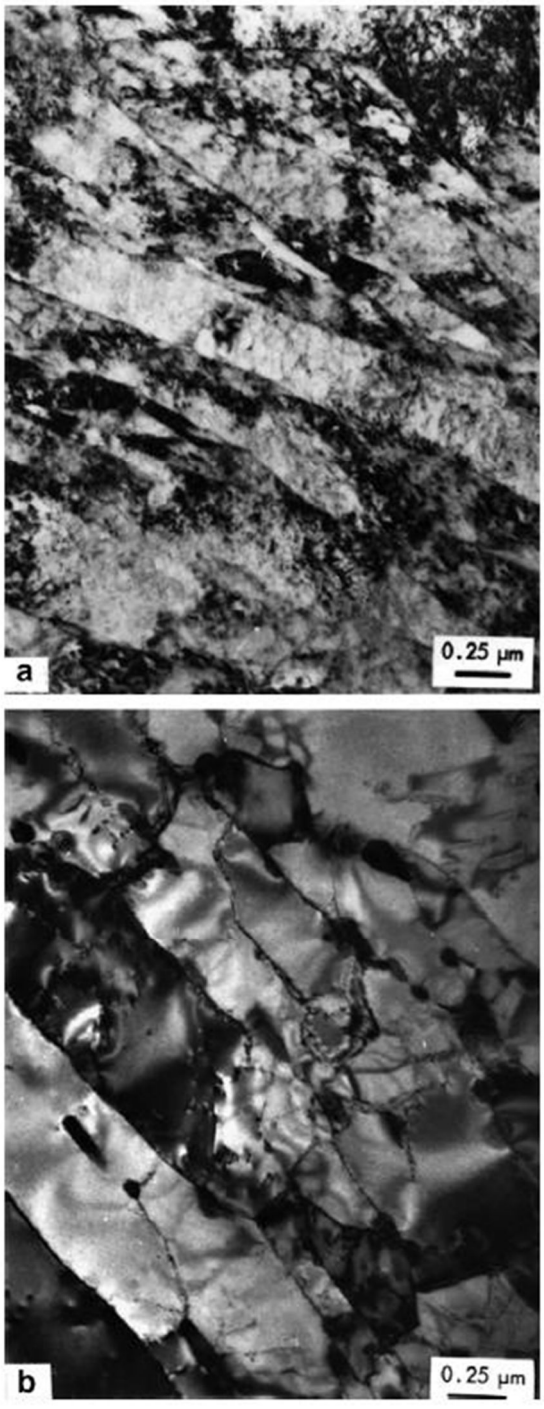

Fig 2.10 Transmission electron microscopy photomicrograph of Sandvik HT9 in the (a) normalized and (b) normalized-and-tempered conditions [9]

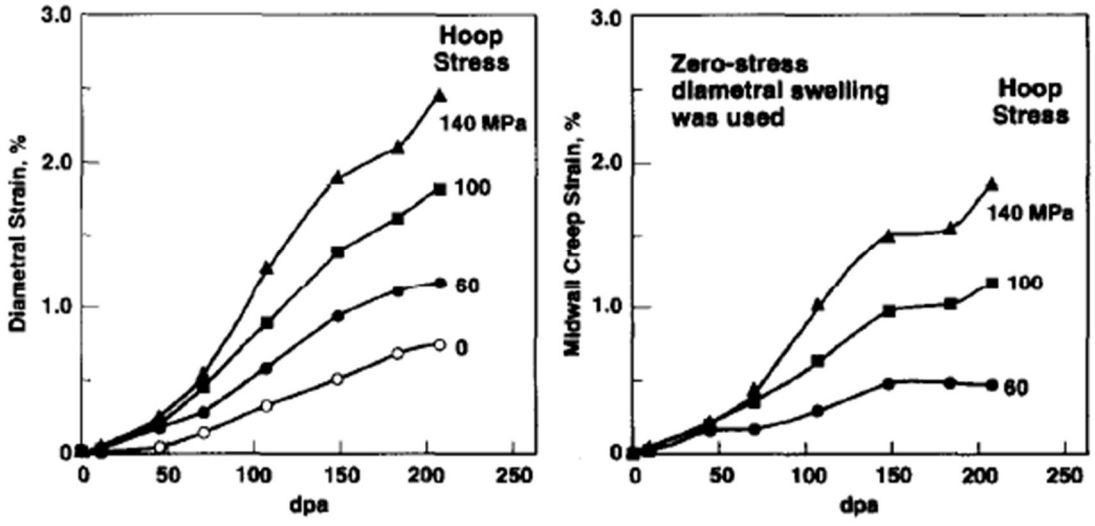

Fig 2.11 Total diametral strains and midwall creep strains for 9Cr-1Mo [13]

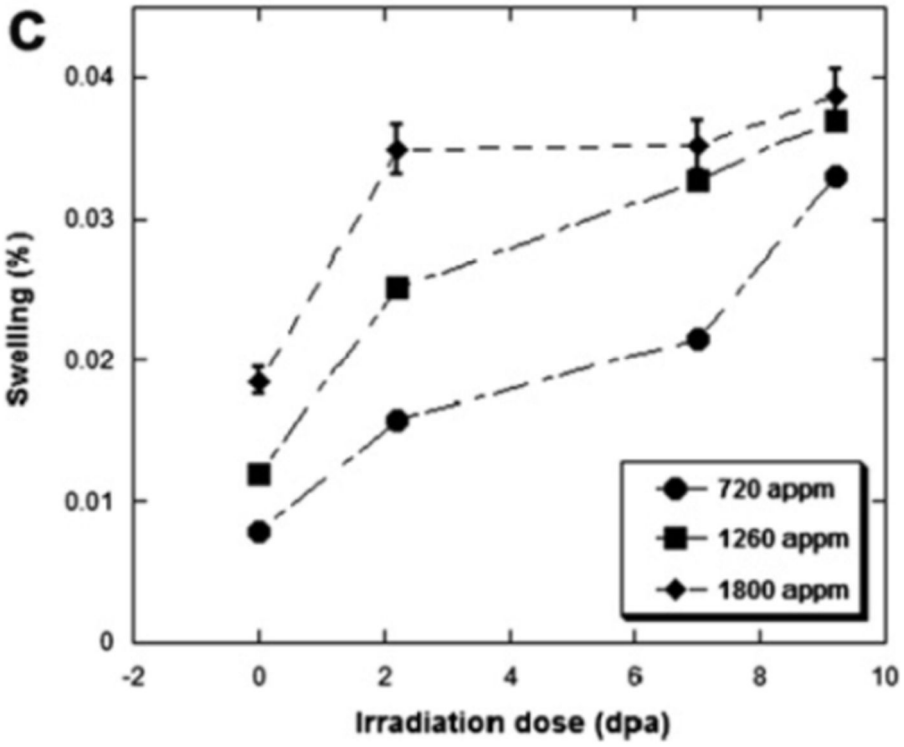

Fig 2.12 Irradiation dose effect on swelling in T91 irradiated at 450℃ [14]

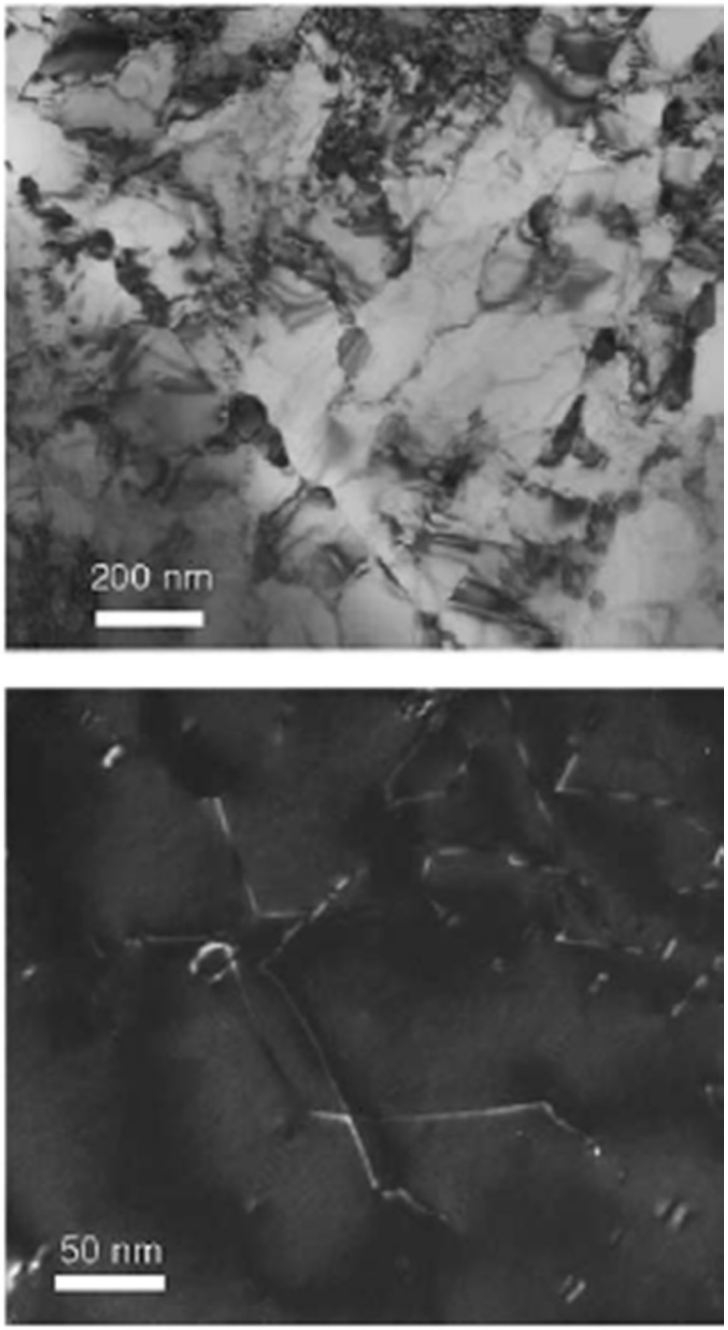

Fig 2.13 The microstructure of unirradiated T91 steels. Upper image (BF images) showing precipitate and martensite lath structures in T91, respectively; lower image (WBDF images) showing the dislocation structures in T91. [15]

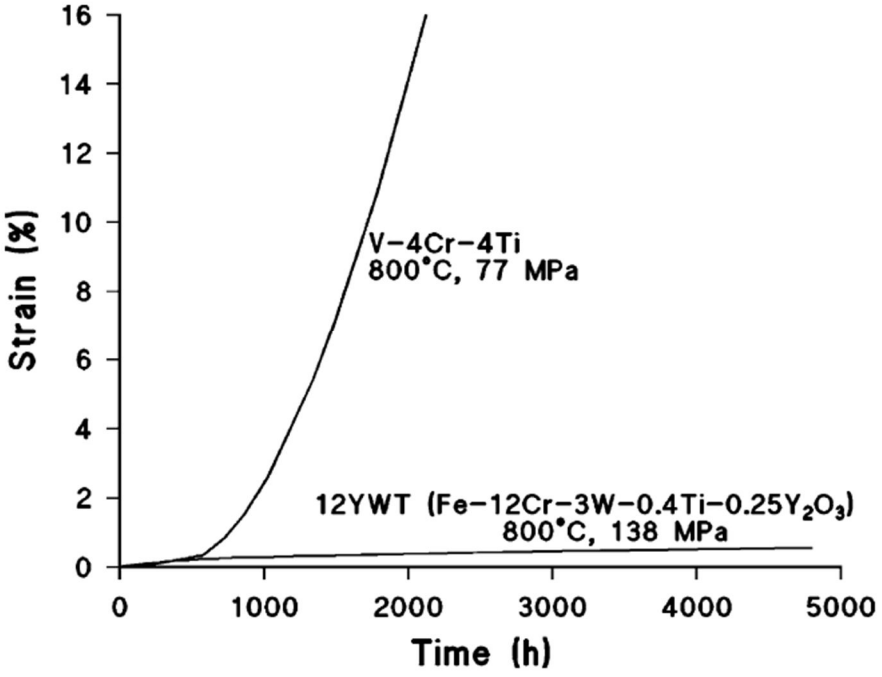

Fig 2.14 A comparison of the creep behavior of the ODS steel 12YWT and the V-4Cr-4Ti alloy [11]

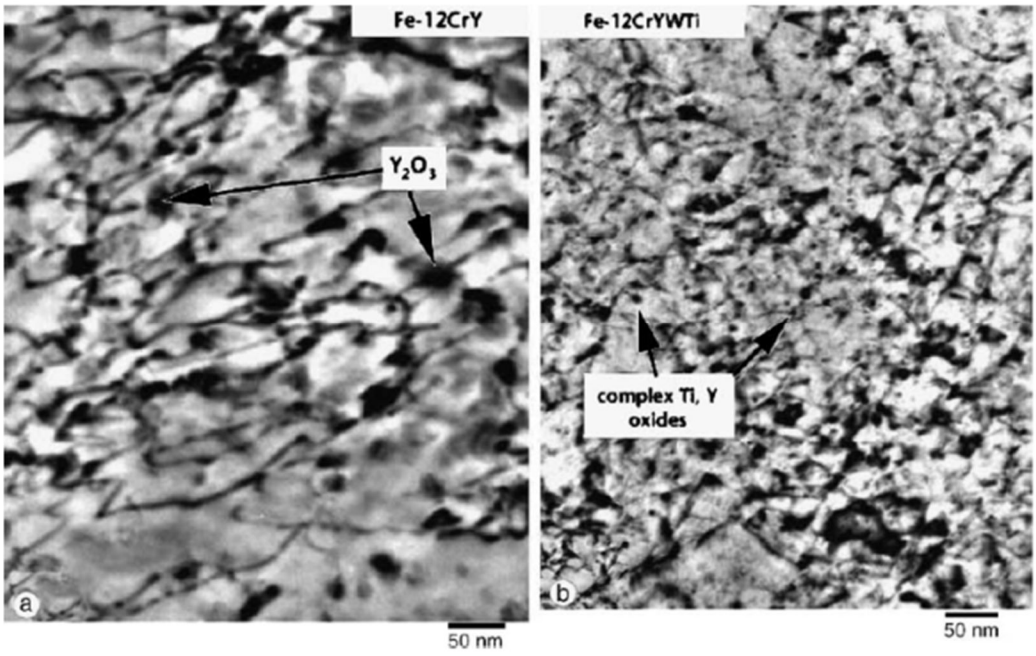

Fig 2.15 Transmission electron micrographs of (a) Fe 12Cr-0.25Y_2O_3(12Y1) and (b) Fe 12Cr-2.5W-0.4Ti-0.25Y_2O_3(12YWT) steels [11]

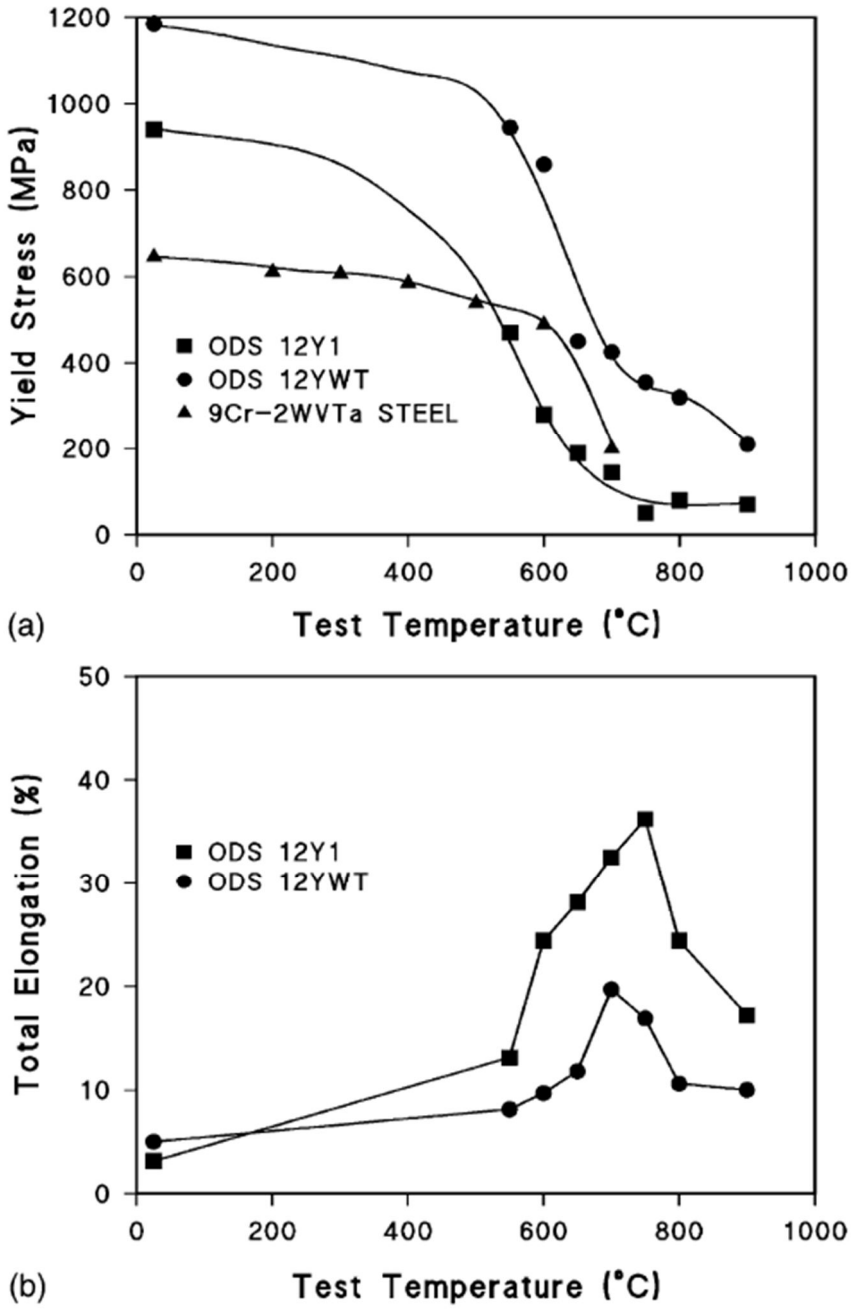

Fig 2.16 (a) The 0.2% yield stress of the 12Y1 and 12YWT ODS steels and the reduced-activation 9Cr-2WVT a steel and (b) the total elongation of the 12Y1 and 12YWT [11]

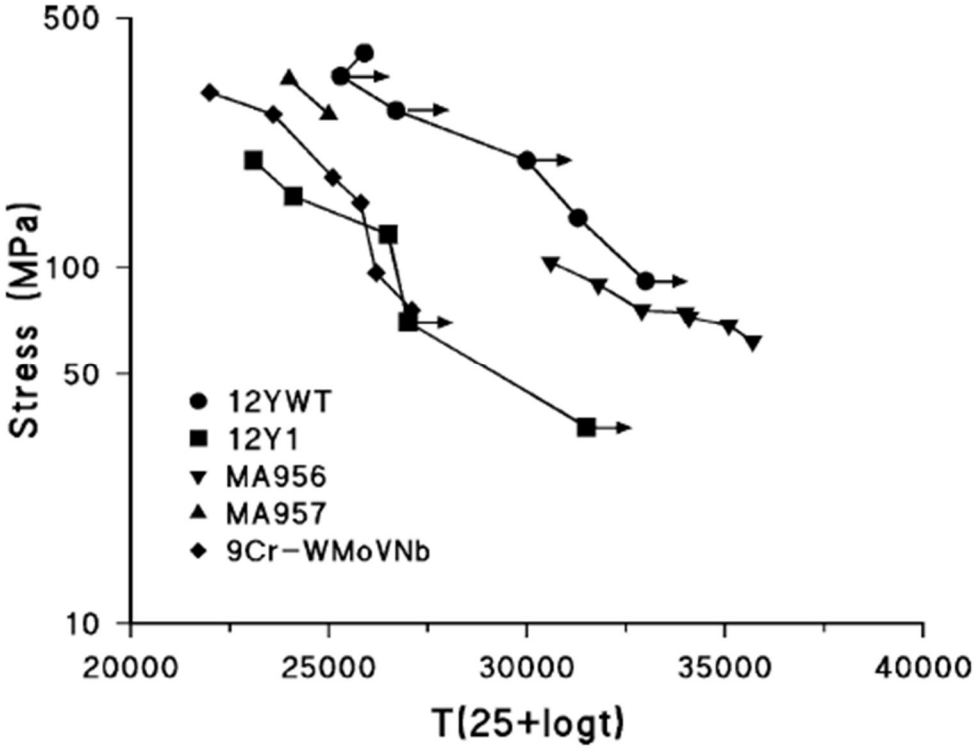

Fig 2.17 Larson-Miller diagram for the creep-rupture strength of four ODS steels and a conventional ferritic/martensitic steel. The arrows indicate that the test is still in progress, or it was discontinued prior to rupture. [11]

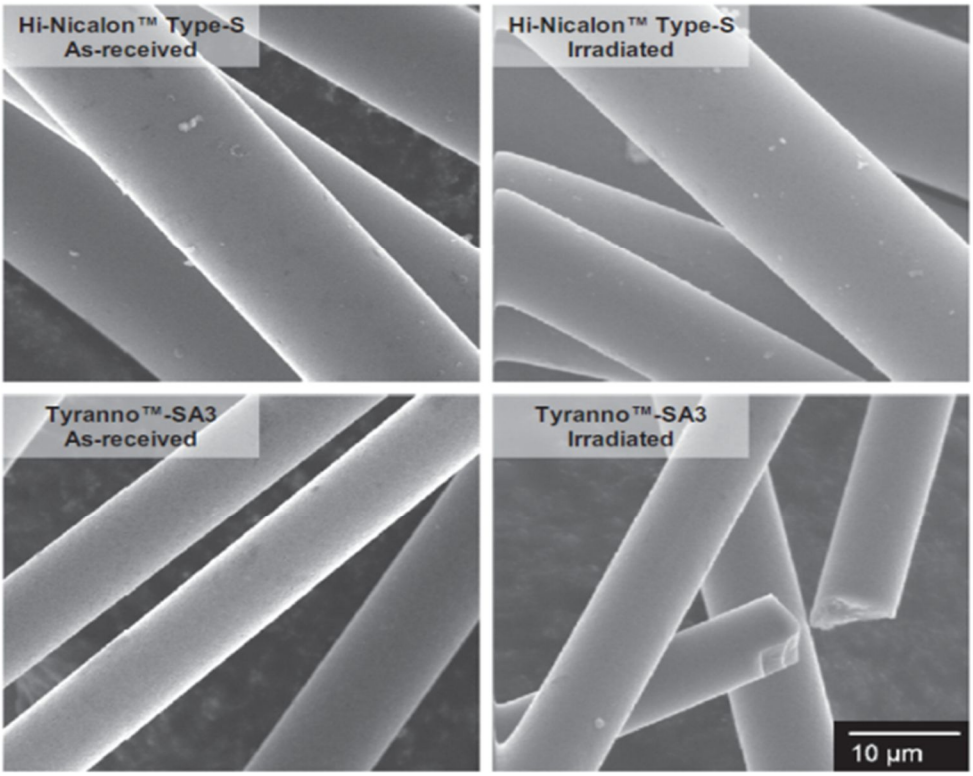

Fig 2.18 Secondary electron images of Hi-Nicalon Type-S and Tyranno-SA3 fibers in as-received and irradiated (910℃, 5.3dpa) conditions [16]

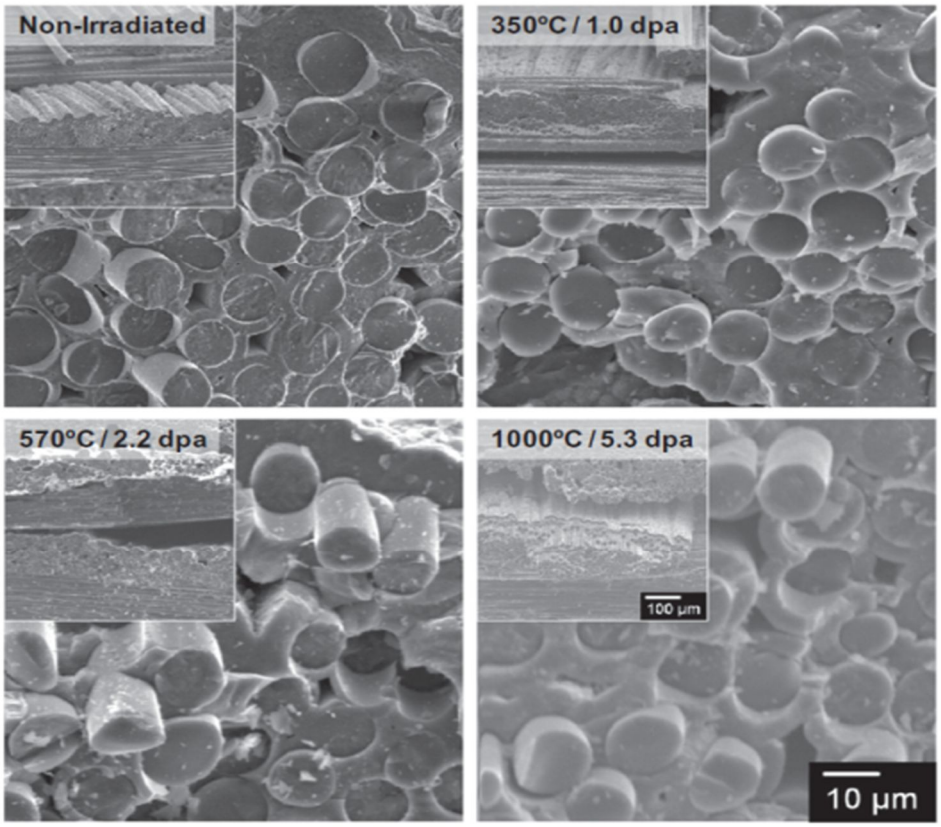

Fig 2.19 Secondary scanning electron images of fracture surfaces of Hi-Nicalon Type-S CVI composites in non-irradiation and various irradiation conditions [16]

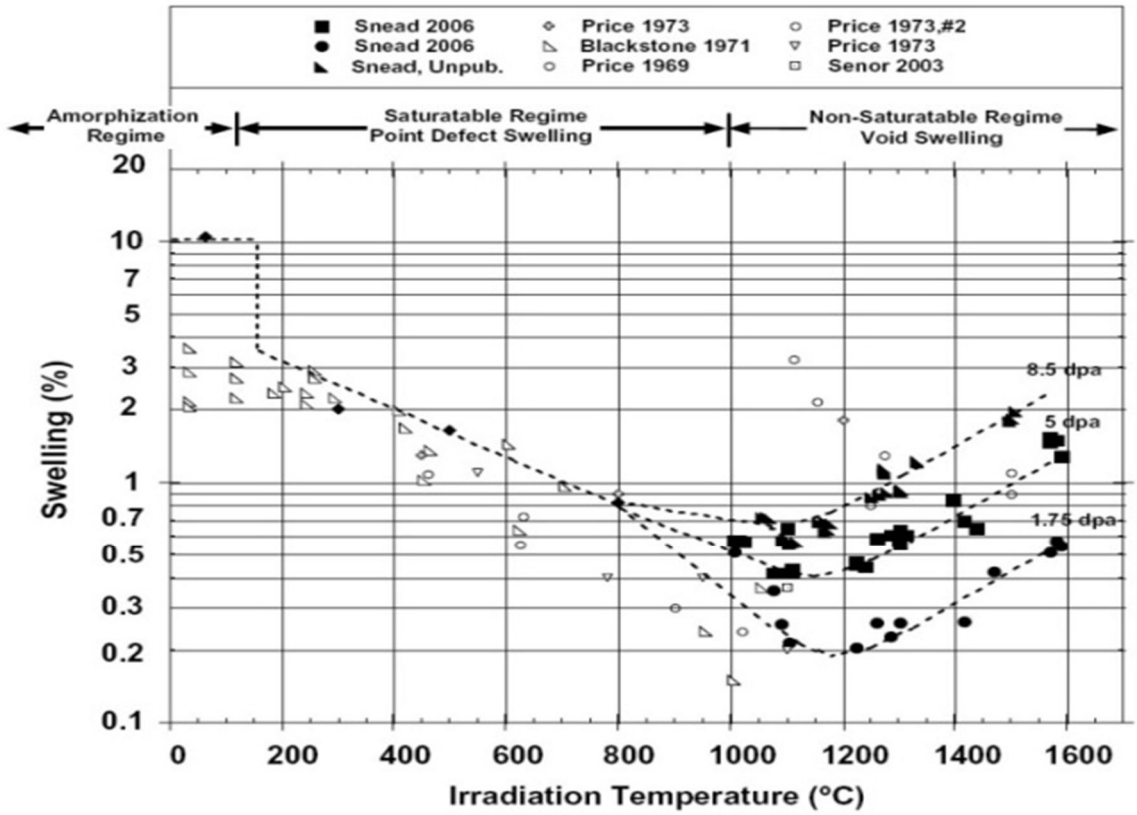

Fig 2.20 Irradiation-induced swelling of SiC to high irradiation temperatures [17]

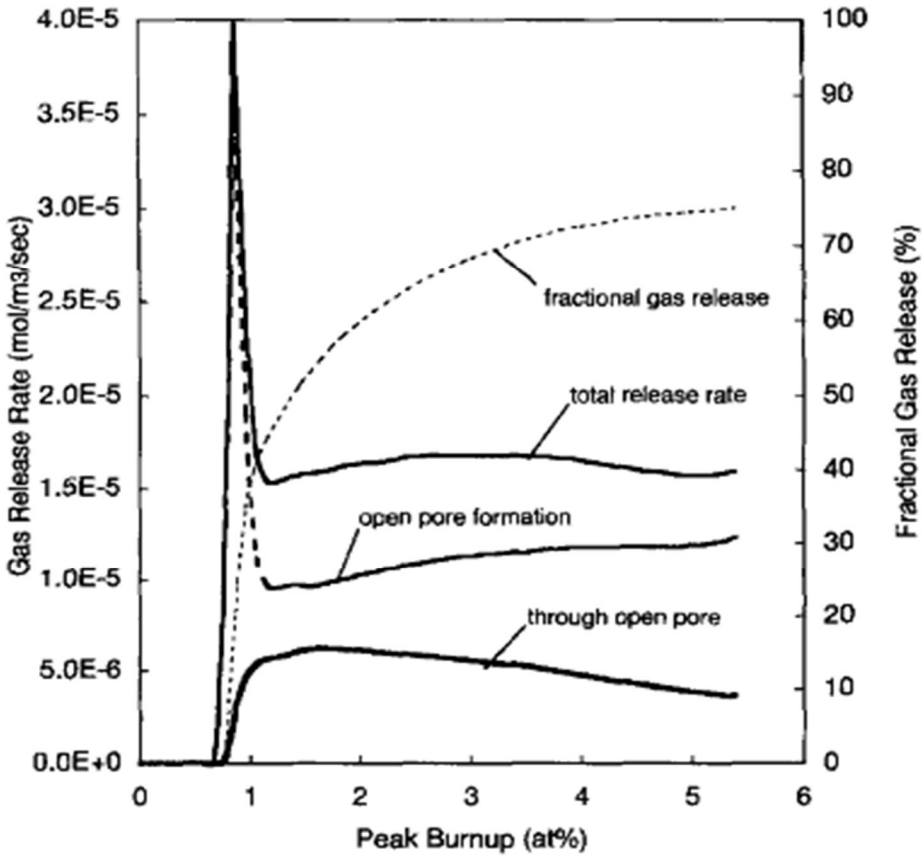

Fig 2.21 Gas release rate of each path and fractional gas release (case-1, 74.5% smear density) [19]

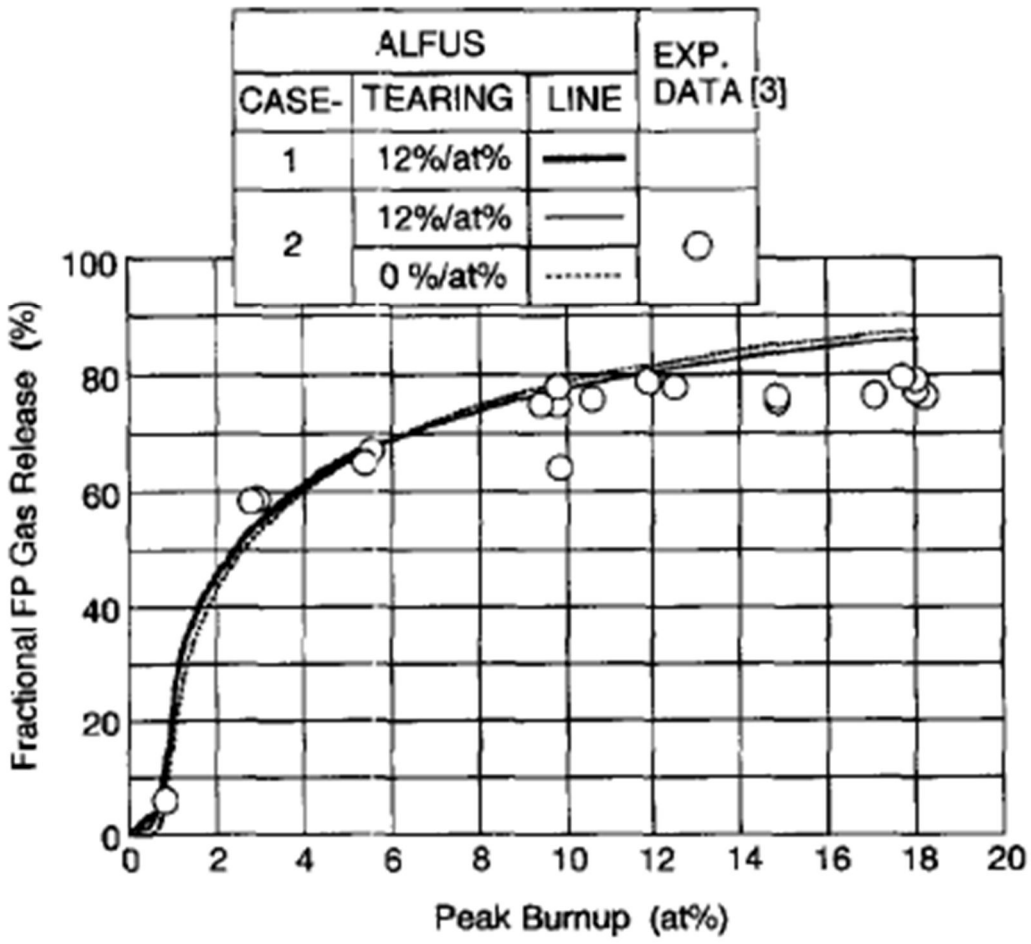

Fig 2.22 FP gas release from the whole fuel slug [19]

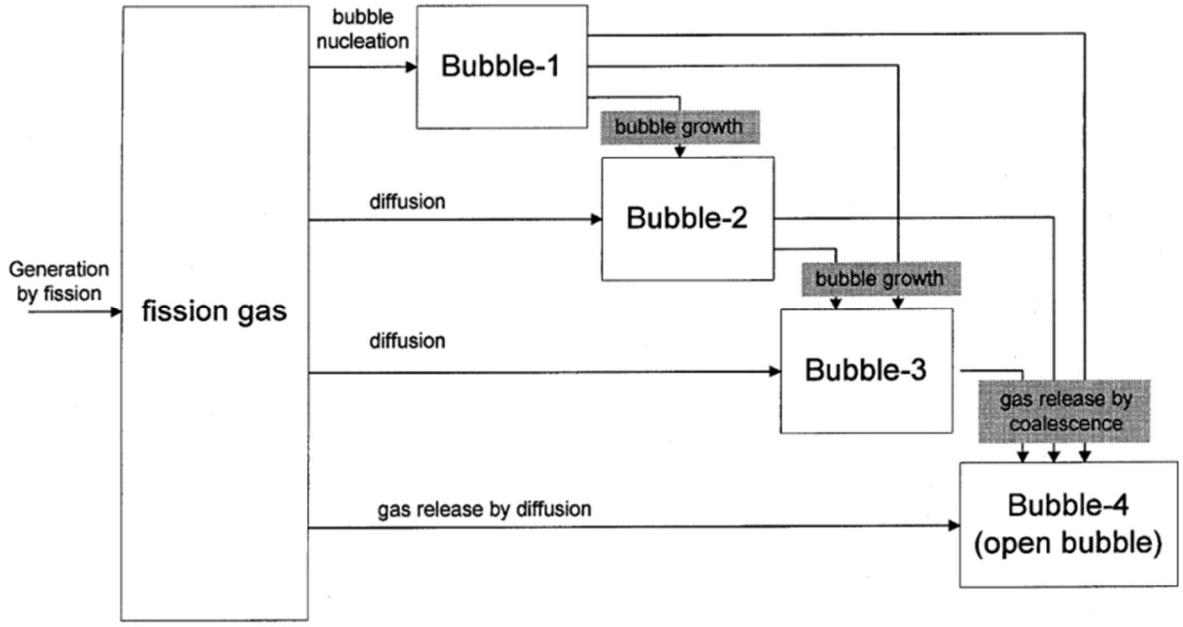

Fig 2.23 Fission gas and bubble movement in the GRSIS model [20]

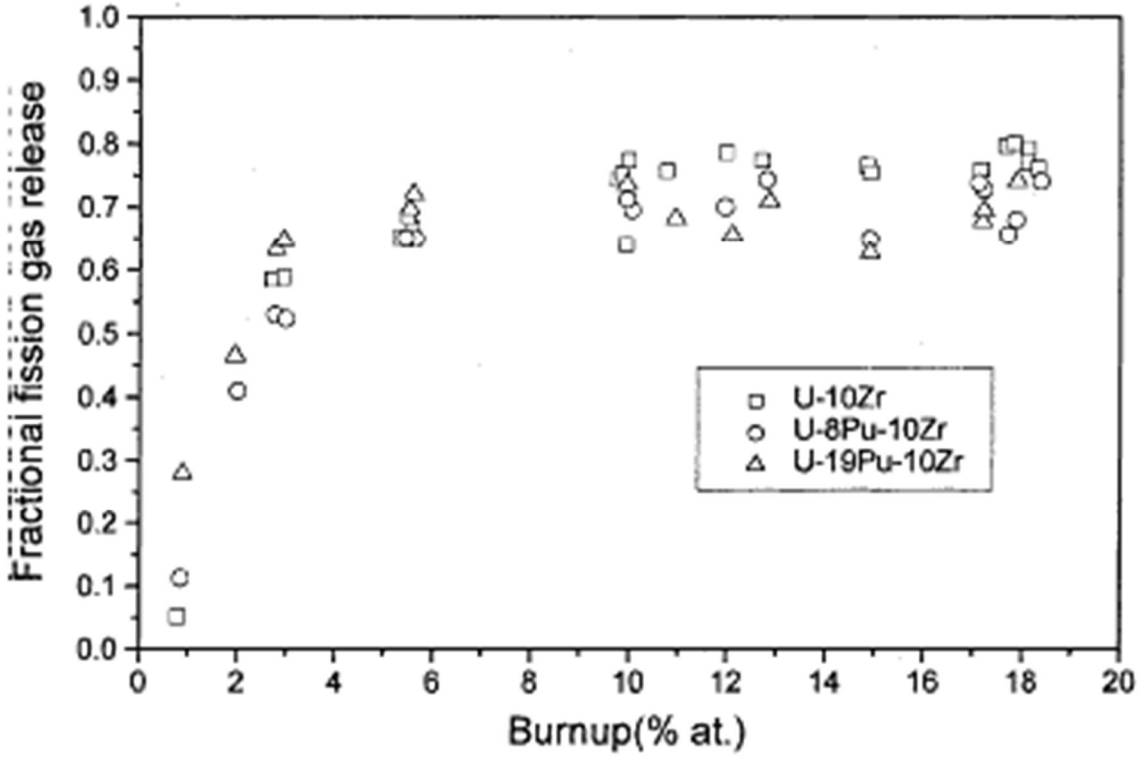

Fig 2.24 Fission gas release of ANL fuel irradiation tests [20]

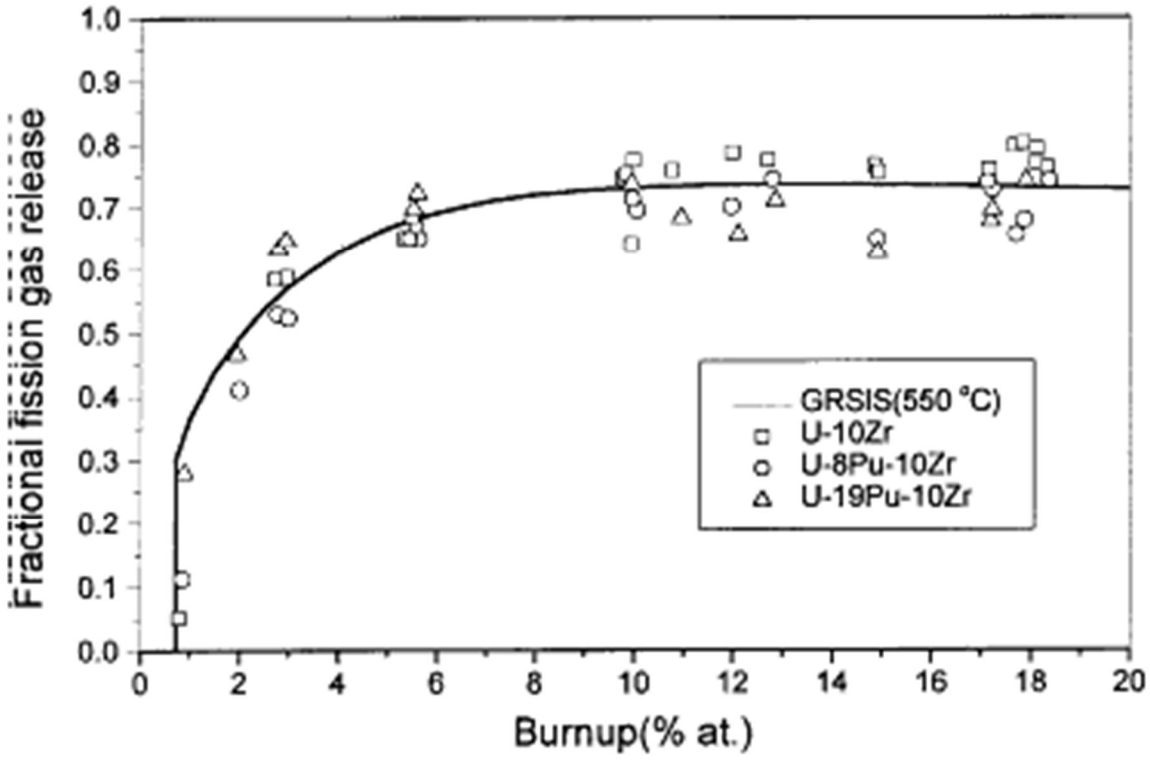

Fig 2.25 Comparison of the GRSIS prediction with the ANL fuel irradiation test results [20]

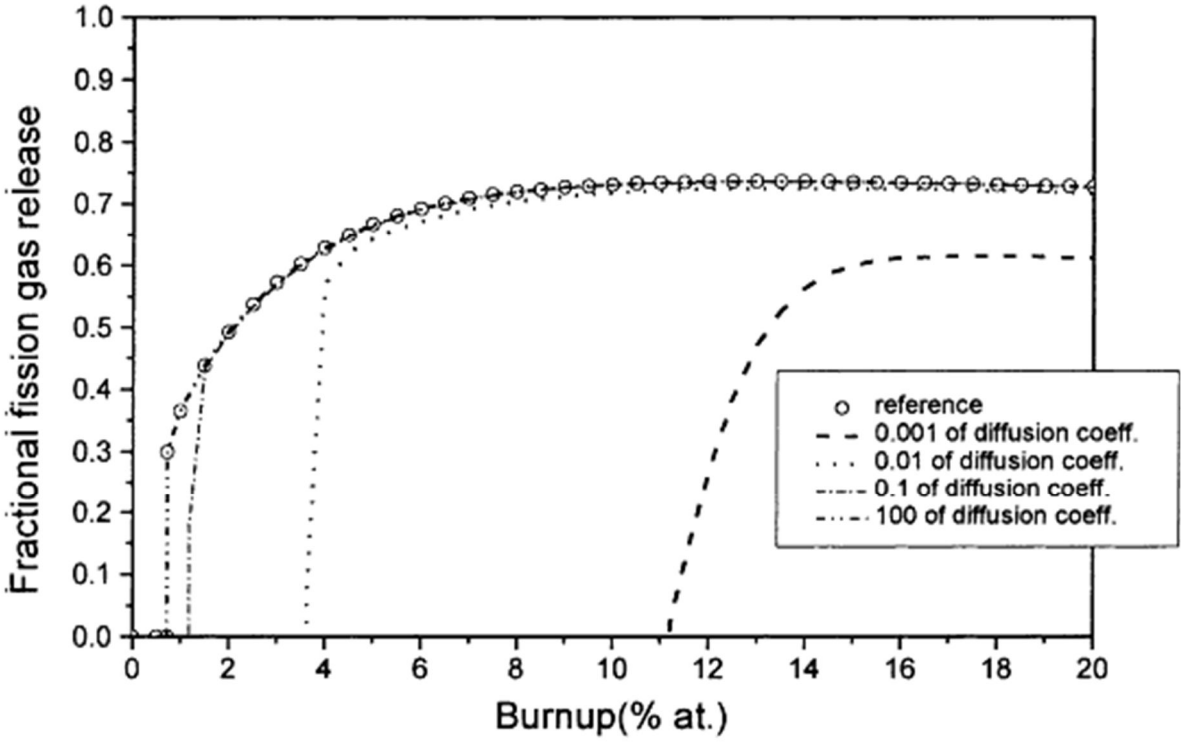

Fig 2.26 Effect of diffusion coefficient upon the fractional fission gas release [20]

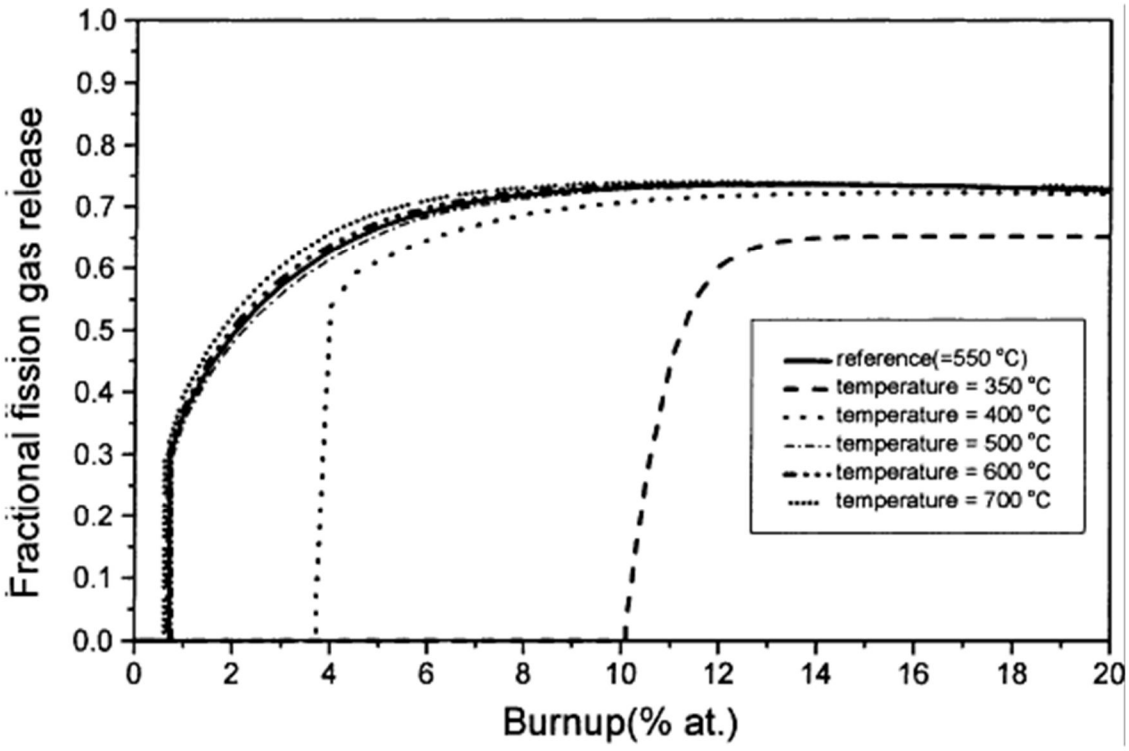

Fig 2.27 Effect of temperature upon the fractional fission gas release [20]

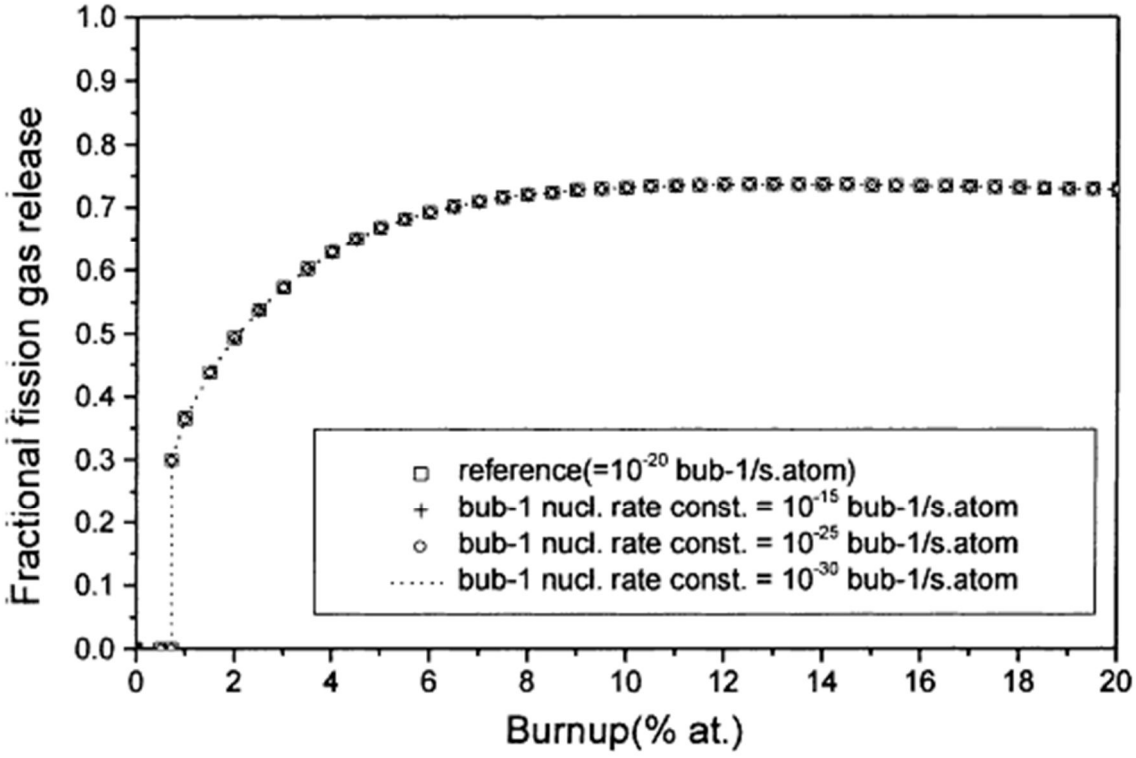

Fig 2.28 Effect of bubble nucleation rate upon the fractional fission gas release [20]

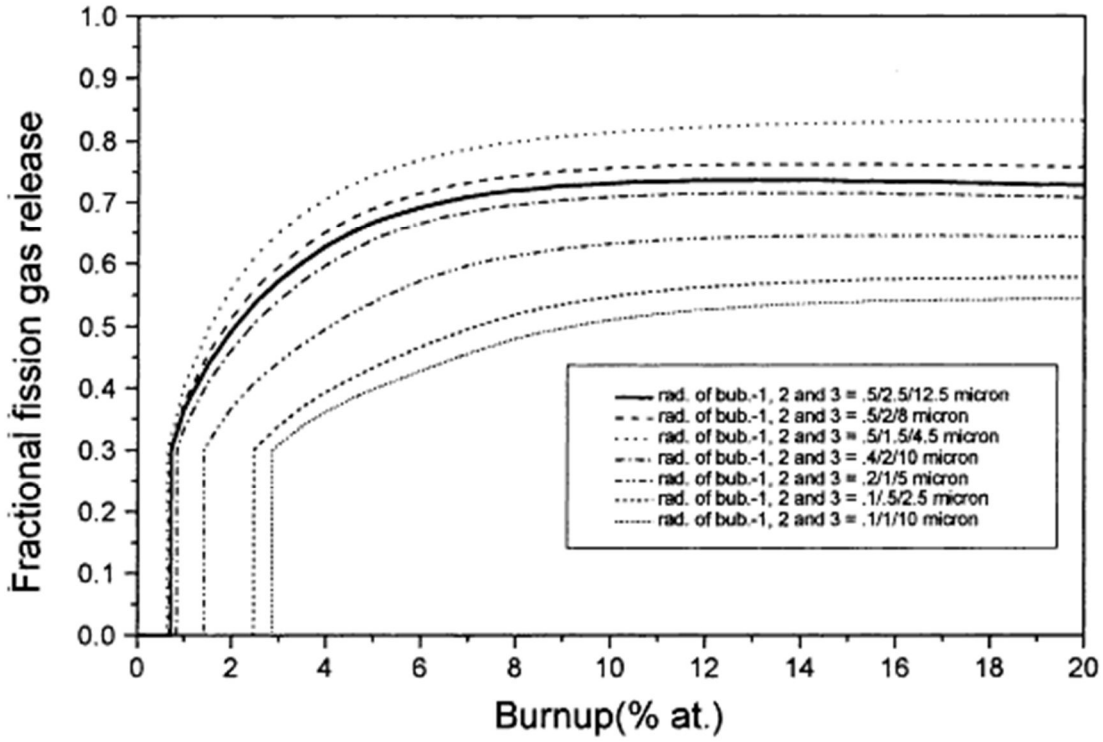

Fig 2.29 Effect of bubble size classification upon the fractional fission gas release [20]

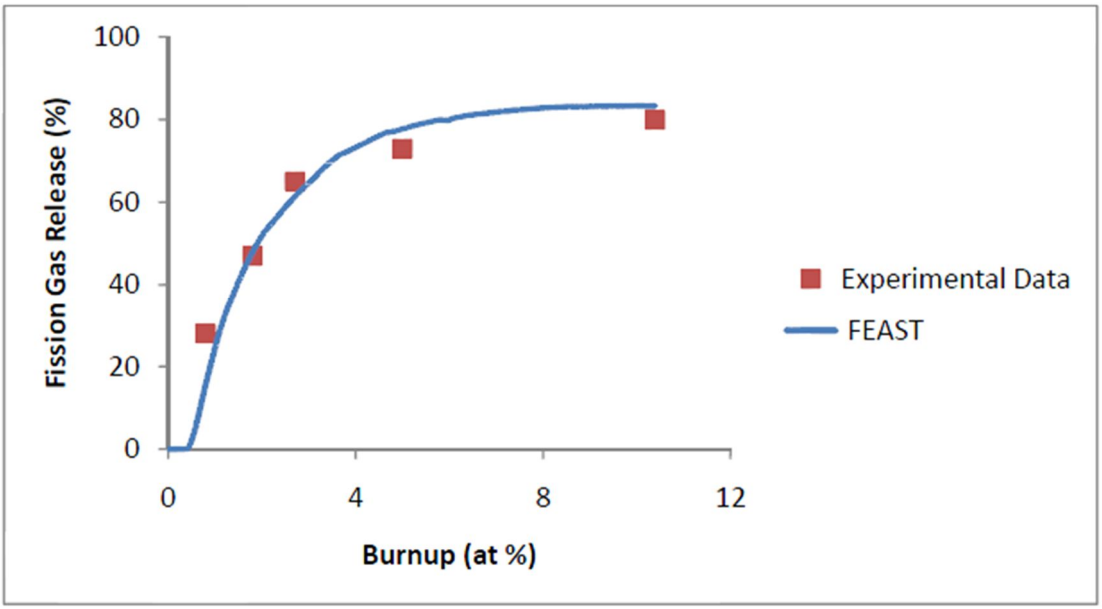

Fig 2.30 Fission gas release behavior of T-654 fuel rod [21]

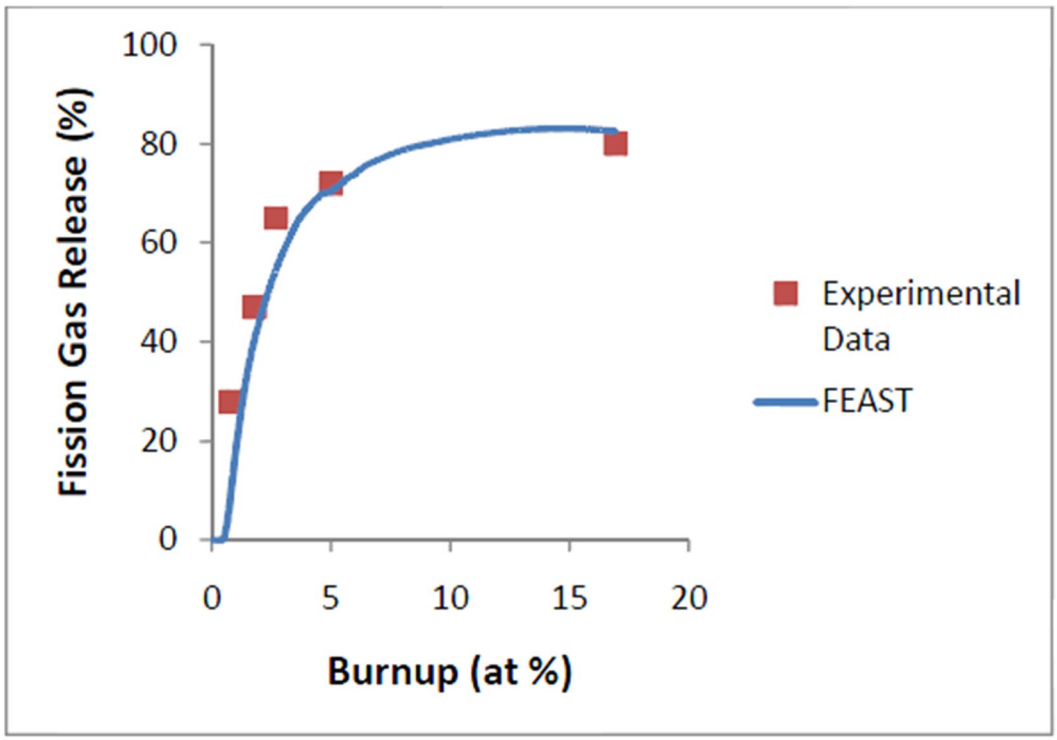

Fig 2.31 Fission gas release behavior of the X425 fuel rod [21]

III. Fuel Cladding Life Prediction

In this chapter, the Case studies are conducted based on chap.2 Literature study. First of all, case study of EBR-Ⅱ research reactor is fulfilled for inspecting effectiveness of every parameter model. The case study of UCFR is conducted after inspecting effectiveness of parameter. Above all, the flowchart is drawn up for checking the parameters to damage in chap 3.1. After that each case study included fraction of fission gas release, dpa, internal pressure, 4 kinds of Stress, thermal creep, irradiation creep, swelling and larson miller parameter. Its contents are as follows.

3.1 Flowchart

The Fig 3.1 shows the flowchart of cladding safety from variety parameters. Various parameters influence Cladding safety. Various parameters include fission gas release, internal pressure, cladding stress, cladding strain, cladding creep rate, temperature, flux, burnup, time, swelling. The Fig 3.1 shows the relationship of those parameters.

3.2 EBR-Ⅱ vs. UCFR

3.2.1 Input Data

At Table 3.1, plenum length, fuel length and fluence are attentively seen. UCFR's plenum and fuel Length are ten times longer than EBR-Ⅱ's. In case of fluence, UCFR's is a hundred times more than EBR-Ⅱ's. [33]

3.2.2 Displacement Per Atom

Definition of dpa (displacements per atom) is the number of times that an atom is displaced for a given fluence. [34]

$$dpa = \sigma_{el} \frac{\Lambda E_n}{4E_d} \phi t$$

$$where\ \sigma_{el} = \text{elastic cross section (3.0barn)},\ \Lambda = 4\mathrm{A}/(1+\mathrm{A})^2 = 0.0689\ (\mathrm{A}=56,\ \text{iron}), \quad (3.1)$$

E_n = neutron energy (0.481MeV), E_d = displacement energy (40eV),

ϕt = fluence (2.94 x 10^{24} n / cm^2)

3.2.3 Fission Gas Release

- EBR-Ⅱ case

GRSIS code(Fission gas release for Metallic fuel) is used on EBR-Ⅱ case. [20]

Using Data are Time = 2080 h = 5.7 y, Burnup = 20% = 190 MWD/t, Cgb1 = 0.4979 x 1027 , Cgb2 = 0.8549 x 1026 , Cgb3 = 0.4226 x 1025 , Cgb4 = 0.1569 x 1028 (atom/m3), FGR = 0.1569 x 1028 (atom/m3), Fraction of FGR = 0.7275 = 73%

- UCFR case

GRSIS code(Fission gas release for Metallic fuel) is used on UCFR case. [20]

Using Data are Period : 26.4 years (9672 days), Fission gas release (atoms/m3) = 0.7336E28, Fraction of fission gas release = 73.16%

3.2.4 Internal Pressure

- EBR-Ⅱ (5.7y) case [35]

$$P_p = \alpha_0 L_f \frac{T_p P_0}{273 L_p} = 19.5 MPa \tag{3.2}$$

EBR 2 fuel rod data is as follows,

where $\mathbf{T_0}$=273K, $\mathbf{P_0}$=1atm=1.013x10^{5}Pa, $\mathbf{P_p}$=plenum pressure at the end of pin life, $\mathbf{L_p}$=plenum length = 0.91m, $\mathbf{L_f}$=fuel length = 0.36m, $\mathbf{T_p}$=plenum temperature = 873K, $\mathbf{V_0}$=$\alpha_0 V_f$, $\mathbf{V_f}$=active fuel volume, **F**=fission gas release fraction = 0.73, **n**=kg·mol fission gas produced/m^3 fuel(4.89x10^{-2}B), **R**=universal gas constant (8317 J/kg·mol·K), $\boldsymbol{\alpha_0}$=1.096 FB(m^3 fission gas at STP/m^3 fuel), **B**=Burnup (MWD/kg) = 20% = 190 MWD/kg

- UCFR (60y) case [35]

$$P_p = \alpha_0 L_f \frac{T_p P_0}{273 L_p} = 39.6 MPa$$

(3.3)

UCFR fuel rod data is as follows,

where T_0=273K, **P_0**=1atm=1.013x10^5Pa, **P_p**=plenum pressure at the end of pin life, **L_p**=plenum length = 7.0m (assumption), **L_f**=fuel length = 3.6m, **T_p**=plenum temperature = 923K, **V_0**=$\alpha_0 V_f$, **V_f**=active fuel volume, **F**=fission gas release fraction = 0.73, **n**=kg·mol fission gas produced/m^3 fuel(4.89x10^{-2}B), **R**=universal gas constant (8317 J/kg·mol·K), **α_0**=1.096 FB(m^3 fission gas at STP/m^3 fuel), **B**=Burnup (MWD/kg) = 29.76% = 282 MWD/kg

3.2.5 Stress(Axial, Hoop, Radial, Effective)

- EBR-Ⅱ (5.7y) case [35]

Axial stress formula is as follows,

$$\sigma_a = \frac{Pr}{2t} \text{ (for a cylinder)} = \frac{19.5\times10^6 \times 0.0022}{2\times 0.00023} = 93.2MPa \tag{3.4}$$

Hoop stress formula is as follows,

$$\sigma_\theta = \frac{Pr}{t} \text{ (for a cylinder)} = \frac{19.5\times10^6 \times 0.0022}{0.00023} = 186.3MPa \tag{3.5}$$

Radial stress formula is as follows,

$$\sigma_r = -\frac{1}{2}P = -9.74MPa \tag{3.6}$$

Effective stress formula is as follows,

$$\begin{aligned}\sigma_e &= \frac{1}{\sqrt{2}}[(\sigma_\theta - \sigma_r)^2 + (\sigma_r - \sigma_a)^2 + (\sigma_a - \sigma_\theta)^2]^{1/2} \\ &= \frac{1}{\sqrt{2}}[(186.5+9.75)^2 + (-9.75-93.3)^2 + (93.3-186.5)^2]^{1/2} \\ &= 169.88MPa\end{aligned} \tag{3.7}$$

EBR 2 fuel rod data is as follows,

where σ_θ = Hoop stress, **P** = Internal pressure = 19.5 Mpa = 19.5 x 10^6 Pa, **r** = inside radius of

the cladding = 0.22 cm = 0.0022 m, **t** = Cladding thickness = 0.023 cm = 0.00023 m, **r/t** = 0.22/0.023 = 9.56 ,

- UCFR (60y) case [35]

Axial stress formula is as follows,

$$\sigma_a = \frac{Pr}{2t} \text{ (for a cylinder)} = \frac{39.7\times10^6\times0.00695}{2\times0.0005} = 261.2MPa \tag{3.8}$$

Hoop stress formula is as follows,

$$\sigma_\theta = \frac{Pr}{t} \text{ (for a cylinder)} = \frac{39.7\times10^6\times0.00695}{0.0005} = 522.5MPa \tag{3.9}$$

Radial stress formula is as follows,

$$\sigma_r = -\frac{1}{2}P = -18.79MPa \tag{3.10}$$

Effective stress formula is as follows,

$$\sigma_e = \frac{1}{\sqrt{2}}[(\sigma_\theta-\sigma_r)^2+(\sigma_r-\sigma_a)^2+(\sigma_a-\sigma_\theta)^2]^{1/2}$$
$$= \frac{1}{\sqrt{2}}[(551.8+19.85)^2+(-19.85-275.9)^2+(275.9-551.8)^2]^{1/2}$$
$$= 468.84MPa$$
(3.11)

UCFR fuel rod data is as follows,

where σ_θ = Hoop stress, P = Internal pressure = 39.7 Mpa = 39.7 x 10^6 Pa, r = inside radius of the cladding = 0.695cm = 0.00695m, t = Cladding thickness = 0.05cm = 0.0005m, r/t = 0.695/0.05 = 13.9

3.2.6 Thermal Creep

- EBR-Ⅱ (5.7y) case [36]

$$\varepsilon_{ps} = \varepsilon_p \left[1 - \exp(-mt)\right] + \dot{\varepsilon}_s t$$
$$where$$
$$P_o(T) = 0.52 - \frac{2647.31}{T}$$
$$P_1(T) = 1.09 - \frac{31.48}{T} \qquad (3.12)$$
$$\varepsilon_p = 0.679\%$$
$$\varepsilon_s = 0.446\%$$

$$t_r \dot{\varepsilon}_s^q = C$$
$$\lambda = \varepsilon_r / \varepsilon_s = \dot{\varepsilon}_{ave} / \dot{\varepsilon}_s$$
$$\varepsilon / \varepsilon_r = 1 - (1 - t / t_r)^{1/\lambda}$$
$$C = 4.48 \times 10^{-5} (\%)$$

where $\varepsilon = 0.679 + 0.446 + 4.48 \times 10^{-5} = 1.125[\%]$, **σ** = effective stress = 169.88Mpa, **T** = temperature (K) = 873K [37]

- UCFR (60y) case [36]

$$\varepsilon_{ps} = \varepsilon_p \left[1 - \exp(-mt)\right] + \dot{\varepsilon}_s t$$
$$where$$
$$P_o(T) = 0.52 - \frac{2647.31}{T}$$
$$P_1(T) = 1.09 - \frac{31.48}{T} \qquad (3.13)$$
$$\varepsilon_p = 0.496\%$$
$$\varepsilon_s = 2.147 \times 10^{10}\%$$

$$t_r \dot{\varepsilon}_s^q = C$$
$$\lambda = \varepsilon_r / \varepsilon_s = \dot{\varepsilon}_{ave} / \dot{\varepsilon}_s$$
$$\varepsilon / \varepsilon_r = 1 - (1 - t / t_r)^{1/\lambda}$$
$$C = 25.536(\%)$$

where $\varepsilon = 0.496 + 2.147 \times 10^{10} + 25.536 = 2.147 \times 10^{10}[\%]$, **σ** = effective stress = 468.84Mpa, **T** = temperature (K) = 873K

3.2.7 Irradiation Creep

- EBR-Ⅱ (5.7y) case [39]

$$\varepsilon_{irr}(\%) = B\sigma_e^n \phi t + DS_0\sigma_e$$
$$= [(-2.9+9.5\times10^{-3}\times873)10^{-26}\times170.02^{1.3}\times2.5\times10^{22}]$$
$$+[6.1\times10^{-6}\times5.721\times10^{-2}\times170.02] = 1.07\% \quad (3.14)$$

where ε_{irr} = irradiation effective creep strain, **Φt** = fast neutron fluence (10^{22} n/cm^2) = 2.5 x 10^{22} n/cm^2 (EBR2), **σ_e** = effective stress (MPa) = 170.02 MPa, **n** = the stress exponent(1.3) for HT9, **B** = creep coefficient of irradiation induction (-2.9+9.5x10^{-3}T(10^{-26}MPa$^{-1.3}$cm^2/n)) for HT9, **D** = swelling enhanced creep coefficient(6.1(10^{-6}MPa^{-1})) for HT9, **S_0** = Swelling (%) = 5.721x10^{-2} % (from GRSIS code output) [38]

- UCFR (60y) case [39]

$$\varepsilon_{irr}(\%) = B\sigma_e^n \phi t + DS_0\sigma_e$$
$$= [(-2.9+9.5\times10^{-3}\times923)10^{-26}\times468.84^{1.3}\times2.57\times10^{24}]$$
$$+[6.1\times10^{-6}\times280.94\times468.84] = 448.31\% \quad (3.15)$$

where ε_{irr} = irradiation effective creep strain, **Φt** = fast neutron fluence(10^{22} n/cm^2) = 2.57 x 10^{24} n/cm^2 (UCFR), **σ_e** = effective stress (MPa) = 495.16Mpa, **n** = the stress exponent(1.3) for HT9, **B** = creep coefficient of irradiation induction (-2.9+9.5x10^{-3}T(10^{-26}MPa$^{-1.3}$cm^2/n)) for HT9, **D** = swelling enhanced creep coefficient(6.1(10^{-6}MPa^{-1})) for HT9, **S_0** = Swelling (%) = 280.94 % (from GRSIS code output) [38]

3.2.8 Swelling

- EBR-Ⅱ (5.7y) case [40]

$$\left(\frac{\Delta V}{V}\right)_{swelling} \propto \left[\phi t\right]^{n}$$

$$\left(\frac{\Delta V}{V}\right) = \frac{V_f - V_0}{V_0}$$

$$\cong (0.01) R\left[\phi t + \frac{1}{\alpha}\ln\left(\frac{1+\exp\left[\alpha\left(\tau-\phi t\right)\right]}{1+\exp\left(\alpha\tau\right)}\right)\right] \quad (3.16)$$

$$= 3.43\times10^{-2}$$

$$= 3.43\%$$

where V_f = final specimen volume, **V_0** = initial specimen volume, **R** = swelling rate parameter in units of % per 10^{22} n/cm^2 (E>0.1MeV) = exp(0.497+0.795β-0.948β^2+0.908β^3-1.49β^4)+1.3exp[-8(β-1.35)^2] = 1.276, **β** = (T-500)/100 = 1.0, **Φt** = neutron fluence in units of 10^{22} n/cm^2 (E>0.1MeV) = 2.5, **α** = curvature parameter in units of (10^{22} n/cm^2)$^{-1}$ = 0.75 (for SS316), **τ** = incubation parameter in units of 10^{22} n/cm^2 (E>0.1MeV) = 6.7705 (for SS316), **T** = cladding temperature (℃) = 600℃ [35]

- UCFR (60y) case [40]

$$\left(\frac{\Delta V}{V}\right)_{swelling} \propto \left[\phi t\right]^{n}$$

$$\left(\frac{\Delta V}{V}\right) = \frac{V_f - V_0}{V_0} \cong$$

$$(0.01) R\left[\phi t + \frac{1}{\alpha}\ln\left(\frac{1+\exp\left[\alpha\left(\tau-\phi t\right)\right]}{1+\exp\left(\alpha\tau\right)}\right)\right] \quad (3.17)$$

$$= 2.809$$

$$= 280.9\%$$

where V_f = final specimen volume, **V_0** = initial specimen volume, **R** = swelling rate parameter in units of % per 10^{22} n/cm^2 (E>0.1MeV) = exp(0.497+0.795β-0.948β^2+0.908β^3-1.49β^4)+1.3exp[-8(β-1.35)^2] = 0.02157, **β** = (T-500)/100 = 1.5, **Φt** = neutron fluence in units of 10^{22} n/cm^2 (E>0.1MeV) = 2.57 x 10^2, **α** = curvature parameter in units of (10^{22} n/cm^2)$^{-1}$ = 0.75 (for SS316), **τ** = incubation parameter in units of 10^{22} n/cm^2 (E>0.1MeV) = 8.0005 (for SS316), **T** = cladding temperature (℃) = 650℃ [35]

3.2.9 Larson Miller Parameter

The Larson-Miller parameter [41] is a means of predicting the lifetime of material vs. time and

temperature using a correlative approach based on the Arrhenius rate equation. The value of the parameter is usually expressed as LMP=T(C + log t) where C is a material specific constant often approximated as 20, t is the time in hours and T is the temperature in Kelvin.

Table 3.3 about life prediction has been derived based on ref. [42]. This experiment is taken effect at 700℃, 150MPa, 150dpa. In this environment, the best performance material is the PNC316. The PNC316 can endure over 30 years according to Table 3.1.

Table 3.1 Input data of EBR2 and UCFR [33]

	EBR-II	UCFR
T_0= Initial temperature	273K	273K
T_p=Plenum temperature	873K	923K
L_p=Plenum length	0.91m	7m (Assumption)
L_f=Fuel length	0.36m	3.6m
P_0= Initial pressure	1atm = 1.013 x 10^5Pa	1atm = 1.013 x 10^5Pa
B = Burnup (MWD/kg)	20% = 190MWD/Kg	29.76% = 282MWD/Kg
Φt = Fast neutron fluence (10^{22} n/cm^2)	2.5 x 10^{22} n/cm^2	2.57 x 10^{24} n/cm^2
r = Inside radius of the cladding	0.22cm = 0.0022m	0.695cm = 0.00695m
t = Cladding thickness	0.023cm = 0.00023m	0.05cm = 0.0005m
Q = Self diffusion	1.23eV for HT9	1.23eV for HT9

Table 3.2 Displacement per atom of EBR2 and UCFR

	dpa(30y)	dpa(60y)
EBR-Ⅱ(5.7y)	31(5.7y)	31(5.7y)
UCFR(FM steel)	394.84	789.67
UCFR(ODS steel)	394.84	789.67
UCFR(SiC/SiC_f composite)	328.03	656.07

Table 3.3. Life prediction at 700℃, 150Mpa, 150dpa

Materials	Estimated stress rupture time (hour)
HT9	949.26948
1.4914	36.576873
EM12	463.42718
FV448	9248.7763
PNC-FMS	57478.666
PNC316	63095734

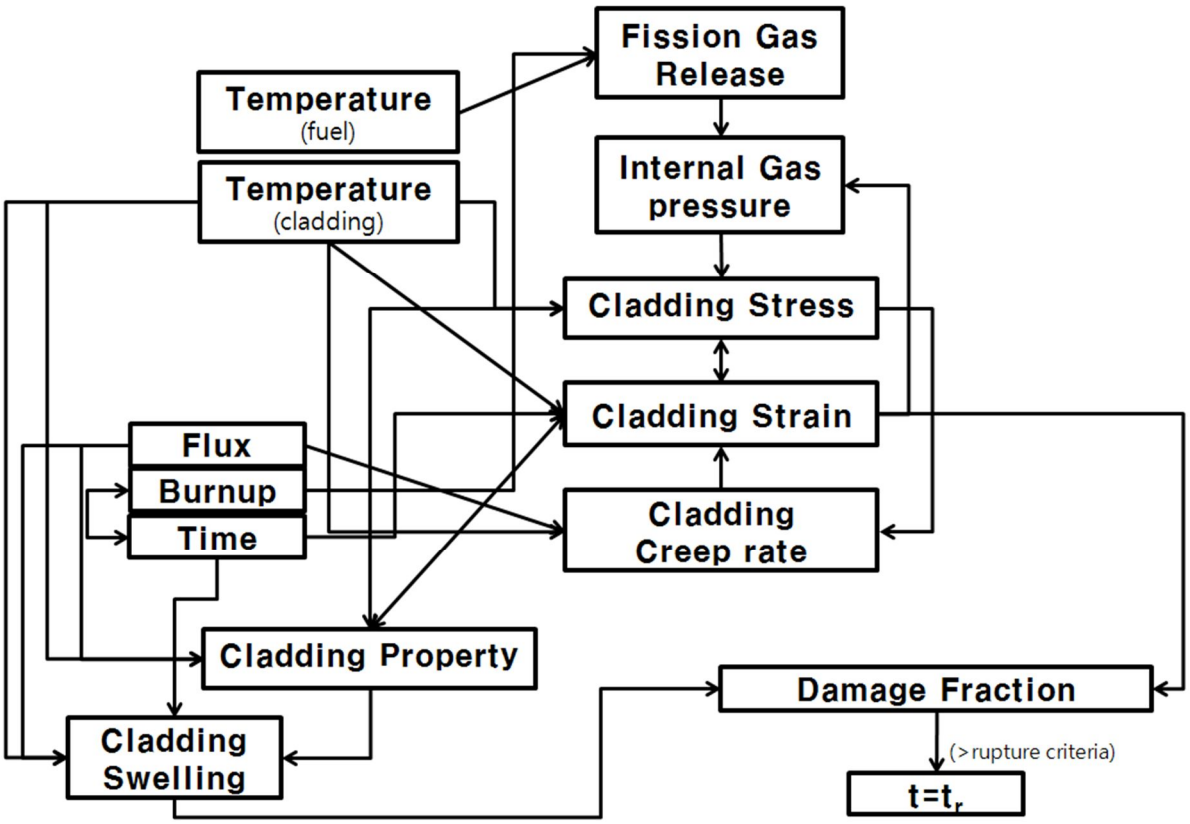

Fig 3.1 The Flowchart of Cladding Safety from variety parameters

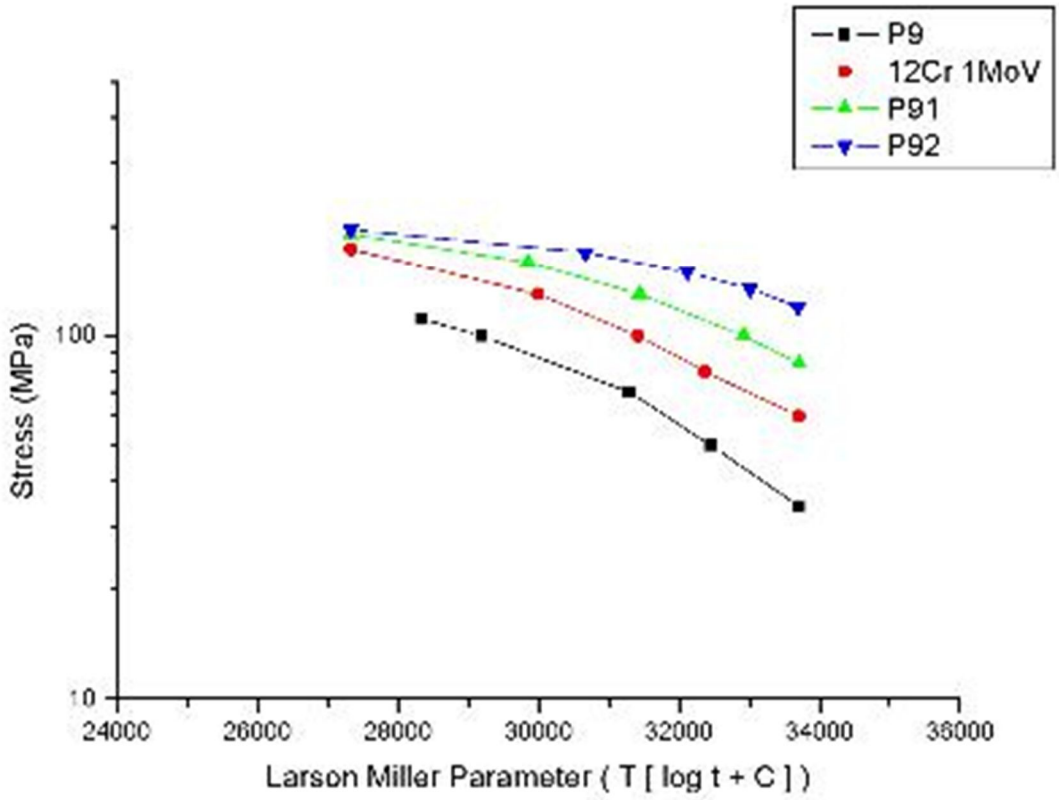

Fig 3.2 The LMP of HT9, P91,P92 at 650℃

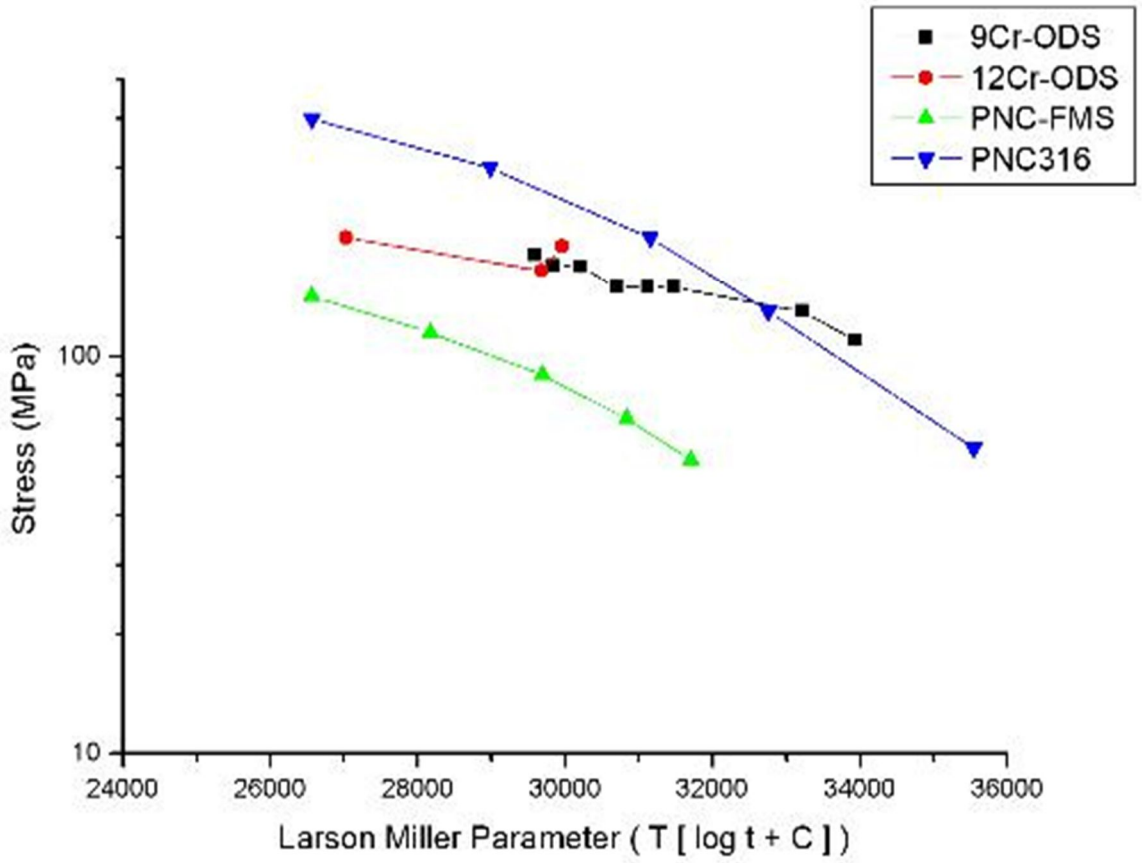

Fig 3.3 The LMP of ODS steel, PNC-FMS, PNC316 at 700 ℃ (75 dpa)

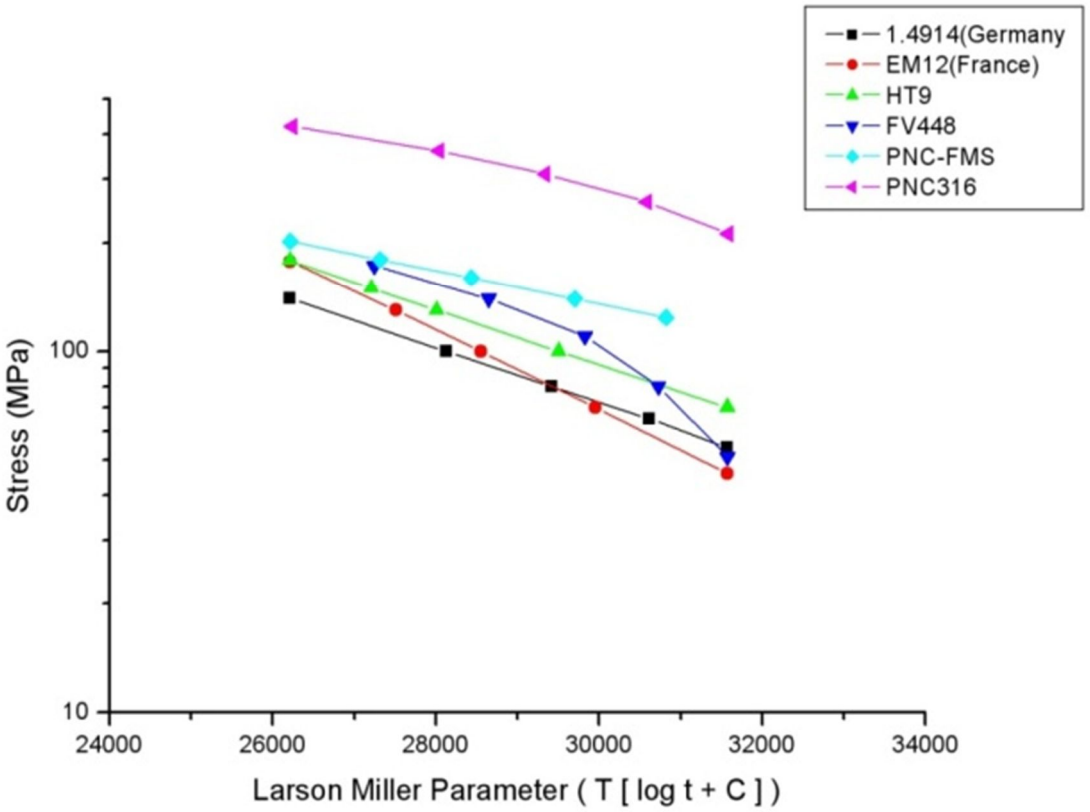

Fig 3.4 The LMP of SFR cladding materials at 650℃ (150 dpa)

IV. Results & Discussion

In this chapter, the results of the case study are summarized, compared and discussed. Above all, the results of case study on EBR-Ⅱ research reactor are satisfied with cladding design criteria described in chapter 1. It proves that the literature study in Chapter 2 is well matched with EBR-Ⅱ case study. Therefore it can be the basis to perform the case study of UCFR. To specifically classify the UCFR environments, two different temperature(600℃ and 650℃), two different operation time with no refueling(30years and 60years), and two different fluence(average and peak) conditions are considered, so in total eight different conditions of UCFR environments, the feasibility study of three different materials, FM steel, ODS and SiC/SiC_f composite are performed. The results show that only SiC/SiC_f composite in the most mild environment (30years, 600℃, average fluence) meets the cladding design criteria. In the same environment (most mild), the results show that the performance of ODS steel is better than that of FM steel. These results are discussed below (in Table 4.4).

4.1 EBR-Ⅱ vs. UCFR

4.1.1 Comparison of various calculated values

Table 4.1 is comparing EBR-Ⅱ case and UCFR case with fission gas release, internal pressure, stress, displacement per atom, thermal creep, irradiation creep and swelling. While EBR2 case is satisfied with cladding design criteria as 1.125(thermal creep), 1.07(irradiation creep), 3.43(swelling), UCFR case is much higher than cladding design criteria. So, FM steel(HT9) cannot be adapted at UCFR environment as cladding materials.

4.2 Conditions of UCFR environments

Table 4.4~4.11 show various environments of UCFR. As mentioned above, only SiC/SiC_f composite in the most mild UCFR environment could meet the cladding design criteria. The thermal creep, irradiation creep and swelling of SiC/SiC_f composite in this environment is 0.0077%, 4.15% and 0.36%, respectively. All but this case, could not satisfy the cladding design criteria. Through the overall case study ODS steel shows better performance than that of FM steel.

In the most mild condition (600℃, 30years, average fluence) the thermal creep, irradiation creep and swelling is 465.03%, 101.85% and 81.03% for FM steel and 367.95%, 14.8% and 5.2% for ODS steel, respectively.

In the most severe condition (650℃, 60years, peak fluence), the thermal creep, irradiation creep and swelling is 2.15×1010%, 543.6% and 280.9% for FM steel and 1089.2%, 63.36% and 21.04% for ODS steel, respectively.

4.3 Life Prediction by LMP

Table 4.2 and 4.3 show the material life prediction evaluated by Larson Miller Parameter. Under non-irradiated environment(expressed as 0dpa), 12YWT(oxide dispersion strengthen) steel have the longest rupture time among six materials (12Y1, 12YWT, MA957, F82H, 9Cr-1Mo, P91) as shown in Table 4.2.

To see the irradiation effects on the rupture life of FM steels, under the same internal pressure(150MPa), and temperature(650℃), additionally neutron damage(corresponding to 150dpa) the life of selective materials are evaluated. The result, show that HT9 have the longest rupture life among three materials (1.4914, EM12 and HT9).

4.4 Discussions

Generally, the refueling time of usual SFR system is designed within 18 months as 1 cycle. Total three times of relocation of loaded fuel is designed in the system. So, normal SFR fuels are located in the system for 54 months. On the other hand, UCFR is designed with no refueling during 30 years of operation period. It is obvious that not only the high burnup but also the large amount of fission gas are caused by the ultra-long operation time of UCFR design and are beyond compare with SFR design. Internal pressure and stress on cladding increase because of amount of fission gas release and extreme environment of UCFR. The UCFR cladding has the thermal creep and irradiation creep because the stress is effected in high temperature and irradiation environment. Also swelling is happened by extreme irradiation environment. The preceding results show that UCFR environment (high temperature, high pressure and high irradiation strength) is too challenging environment for materials. As a results, the most possible concept of UCFR environment is 30y, 600℃, average fluence(2.29×10^{24}n/cm^2) among 8 concept of UCFR environment. The others (FM steels, ODS steels) are not allowed in the aforementioned environment, only SiC/SiC$_f$ composite is satisfied with the design criteria (Table 4.4). Therefore SiC/SiC$_f$ composite can be used as UCFR cladding material. However, welding/joining of SiC/SiC$_f$ composite needed more experience and skills.

When the use metal or alloy cladding for UCFR is needed, the vented fuel concept (Fig 4.9) can be one of the options. Vented fuel that allows only fission gases to escape from fuel pins is greatly preferred from radiological safety considerations over venting designs that allow other fission products to also escape. The vented fuel concept along with radiological aspects of fission gas venting are evaluated, and the thermal-hydraulic performance of the most-promising venting scheme is modeled.[45] Since the required gas plenum length is generally proportional to the fuel discharge burnup, the penalties could be significant in the UHBF(Ultra-High Burnup Fast Reactor). Venting the released fission gases and helium from the fuel pin into the reactor primary coolant flow will maintain low cladding stresses at high burnup as well as decrease plant capital cost due to a significant reduction in reactor vessel height (fuel length is reduced as plenum volume is reduced). [44] A vented inverted fuel assembly design is proposed for a SFR which meets all the design criteria for materials, thermal-hydraulic and venting performance. In creating this design a list of most troublesome nuclides with regard to their potential release has been proposed and the design accomplished accommodating their characteristics. Finally, it has been found that venting can provide a least a 20°C increase in the coolant core outlet temperature with the same mechanical performance (based on a Larson-Miller parameter analysis). This means an increase in plant thermal efficiency of at least 1%. [43] Consequently, the target burnup of the UHBF might be impractical without venting the fission gases from the fuel during irradiation. Numerous issues pertaining to fission gas venting to coolant will need to be addressed. These include vent reliability during normal and off-normal operations, fuel pin

fabrication costs, plant design for increased primary system leak tightness and radiological hazard control. If vented fuel is possible, it makes total strain become smaller. Therefore the safe of cladding will be improved, the cladding may use 60 years. [45]

Regarding fission gas release, Life-Metal code, Stars and Alfus model, Ogres model are considered. But fuel is not metallic fuel or reactor environment is not FBR. So we can chose the GRSIS model, the fuel of this model is metallic fuel and reactor environment is FBR.

There are models(Minimum commitment method(MCM) and Theta projection method(TPM)) of thermal creep. But these models have the errors comparing with experimental data. So we use Garafalo model at primary and steady-state creep regimes and Monkman–Grant model at tertiary creep regime. During life prediction, every model has the material constants which are made by experiment. But there are no experiments similar to UCFR environment. Material constants are not accurate, so we could have small errors.

Table 4.1 Life Prediction Calculation of EBR2 and UCFR

	EBR-II (5.7y) **FM steel**	**UCFR (30y)** **FM steel**
Fraction of fission gas release (%)	73	73
Internal pressure (MPa)	19.48	37.58
Axial stress (MPa)	93.16	261.23
Hoop stress (MPa)	186.33	522.47
Radial stress(MPa)	-9.74	-18.79
Effective stress (MPa)	169.87	468.84
Displacement Per Atom(dpa)	31	394.84
Thermal creep (%)	1.125	465.03
Irradiation creep (%)	1.07	101.85
Swelling (%)	3.43	81.03

Table 4.2 Materials Life Prediction by LMP at 150MPa, 650°C

Materials	Prediction of time to rupture (h)
12Y1	39.19
12YWT	4.2E+08
MA957	860983
F82H	1475.75
9Cr-1Mo	896.04
P91	1.1E+08
1.4914 (150 dpa)	1005
EM12 (150 dpa)	14611
HT9 (150 dpa)	31114.1

Table 4.3 Materials Life Prediction by LMP at 150MPa, 700°C

Materials	Prediction of time to rupture (h)
12Y1	1.68
12YWT	7836855
MA957	22147.5
F82H	52.66
9Cr-1Mo	32.8
P91	2300211
1.4914 (150 dpa)	36.58
EM12 (150 dpa)	463.43
HT9 (150 dpa)	949.27

Table 4.4 Comparison of various calculated values (600℃/30years/Average fluence)

	EBR-II FM steel	**UCFR FM steel**	**UCFR ODS steel**	**UCFR SiC/SiC_f composite**
Fraction of fission gas release (%)	73	79.99	79.99	79.99
Internal pressure (MPa)	19.48	43.6	43.6	43.6
Axial stress (MPa)	93.16	303	303	303
Hoop stress (MPa)	186.33	606	606	606
Radial stress(MPa)	-9.74	-21.8	-21.8	-21.8
Effective stress (MPa)	169.87	543.8	543.8	543.8
Displacement Per Atom(dpa)	31	394.84	394.84	328.03
Thermal creep (%)	2.03	465.03	367.95	0.0077
Irradiation creep (%)	1.07	101.85	14.8	4.15
Swelling (%)	3.43	81.03	5.2	< 0.36

Table 4.5 Comparison of various calculated values (600℃/30years/Peak fluence)

	UCFR FM steel	**UCFR ODS steel**	**UCFR SiC/SiC_f composite**
Fraction of fission gas release (%)	79.99	79.99	79.99
Internal pressure (MPa)	43.6	43.6	43.6
Axial stress (MPa)	303	303	303
Hoop stress (MPa)	606	606	606
Radial stress(MPa)	-21.8	-21.8	-21.8
Effective stress (MPa)	543.8	543.8	543.8
Displacement Per Atom (dpa)	799	799	663.82
Thermal creep (%)	465.04	367.95	0.0077
Irradiation creep (%)	206.11	29.96	8.4
Swelling (%)	163.97	10.52	< 0.36

Table 4.6 Comparison of various calculated values (600℃/60years/Average fluence)

	UCFR FM steel	**UCFR ODS steel**	**UCFR SiC/SiC_f composite**
Fraction of fission gas release (%)	79.99	79.99	79.99
Internal pressure (MPa)	43.6	43.6	43.6
Axial stress (MPa)	303	303	303
Hoop stress (MPa)	606	606	606
Radial stress(MPa)	-21.8	-21.8	-21.8
Effective stress (MPa)	543.8	543.8	543.8
Displacement Per Atom (dpa)	789.67	789.67	656.07
Thermal creep (%)	930.07	735.9	0.0154
Irradiation creep (%)	203.7	29.61	8.3
Swelling (%)	162.06	10.39	< 0.36

Table 4.7 Comparison of various calculated values (600℃/60years/Peak fluence)

	UCFR FM steel	**UCFR ODS steel**	**UCFR SiC/SiC_f composite**
Fraction of fission gas release (%)	79.99	79.99	79.99
Internal pressure (MPa)	43.6	43.6	43.6
Axial stress (MPa)	303	303	303
Hoop stress (MPa)	606	606	606
Radial stress(MPa)	-21.8	-21.8	-21.8
Effective stress (MPa)	543.8	543.8	543.8
Displacement Per Atom (dpa)	1598	1598	1327.63
Thermal creep (%)	930.07	735.9	0.0154
Irradiation creep (%)	412.22	59.93	16.8
Swelling (%)	327.95	21.04	< 0.36

Table 4.8 Comparison of various calculated values (650℃/30years/Average fluence)

	UCFR FM steel	**UCFR ODS steel**	**UCFR SiC/SiC_f composite**
Fraction of fission gas release (%)	79.99	79.99	79.99
Internal pressure (MPa)	43.6	43.6	43.6
Axial stress (MPa)	303	303	303
Hoop stress (MPa)	606	606	606
Radial stress(MPa)	-21.8	-21.8	-21.8
Effective stress (MPa)	543.8	543.8	543.8
Displacement Per Atom (dpa)	394.84	394.84	328.03
Thermal creep (%)	2053.72	544.6	0.0321
Irradiation creep (%)	119.08	15.56	4.39
Swelling (%)	69.41	5.2	< 0.36

Table 4.9 Comparison of various calculated values (650℃/30years/Peak fluence)

	UCFR FM steel	**UCFR ODS steel**	**UCFR SiC/SiC_f composite**
Fraction of fission gas release (%)	79.99	79.99	79.99
Internal pressure (MPa)	43.6	43.6	43.6
Axial stress (MPa)	303	303	303
Hoop stress (MPa)	606	606	606
Radial stress(MPa)	-21.8	-21.8	-21.8
Effective stress (MPa)	543.8	543.8	543.8
Displacement Per Atom (dpa)	799	799	663.82
Thermal creep (%)	2053.72	544.6	0.0321
Irradiation creep (%)	240.97	31.68	8.88
Swelling (%)	140.46	10.52	< 0.36

Table 4.10 Comparison of various calculated values (650℃/60years/Average fluence)

	UCFR FM steel	**UCFR ODS steel**	**UCFR SiC/SiC_f composite**
Fraction of fission gas release (%)	79.99	79.99	79.99
Internal pressure (MPa)	43.6	43.6	43.6
Axial stress (MPa)	303	303	303
Hoop stress (MPa)	606	606	606
Radial stress(MPa)	-21.8	-21.8	-21.8
Effective stress (MPa)	543.8	543.8	543.8
Displacement Per Atom (dpa)	789.67	789.67	656.07
Thermal creep (%)	4107.43	1089.2	0.0641
Irradiation creep (%)	238.16	31.31	8.78
Swelling (%)	138.82	10.39	< 0.36

Table 4.11 Comparison of various calculated values (650℃/60years/Peak fluence)

	UCFR FM steel	**UCFR ODS steel**	**UCFR SiC/SiC_f composite**
Fraction of fission gas release (%)	79.99	79.99	79.99
Internal pressure (MPa)	43.6	43.6	43.6
Axial stress (MPa)	303	303	303
Hoop stress (MPa)	606	606	606
Radial stress(MPa)	-21.8	-21.8	-21.8
Effective stress (MPa)	543.8	543.8	543.8
Displacement Per Atom (dpa)	1598	1598	1327.89
Thermal creep (%)	2.15×10^{10}	1089.2	0.0641
Irradiation creep (%)	543.6	63.36	17.76
Swelling (%)	280.9	21.04	0.36

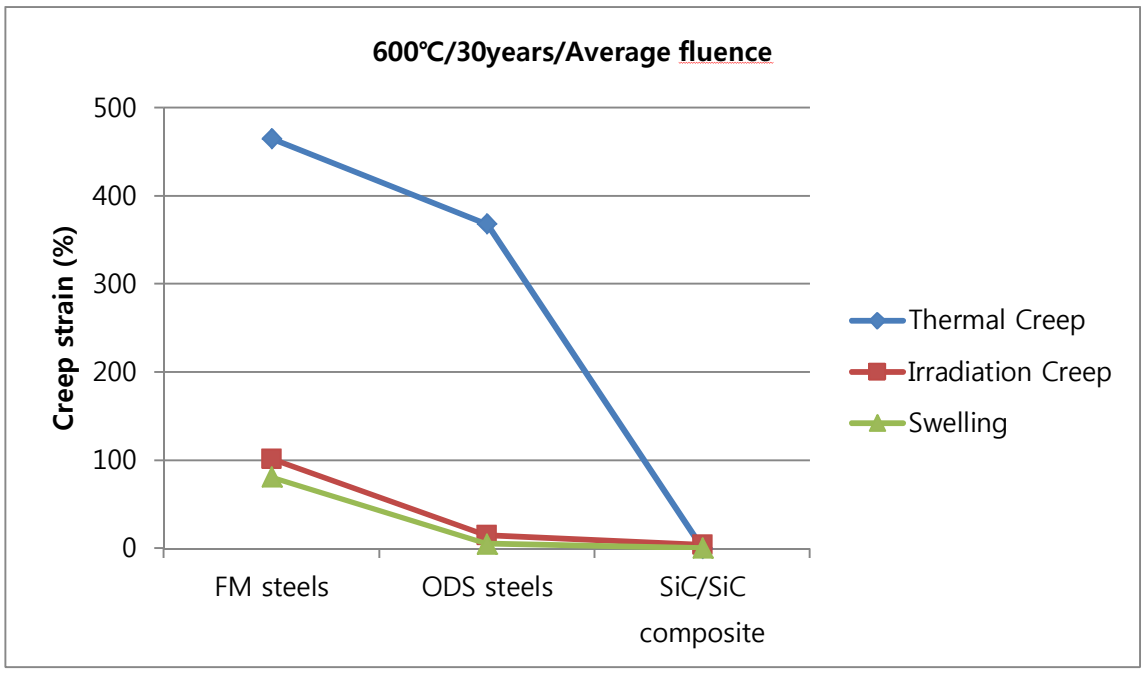

Fig 4.1 Comparing creep strain at 600℃/30years/Avg.fluence

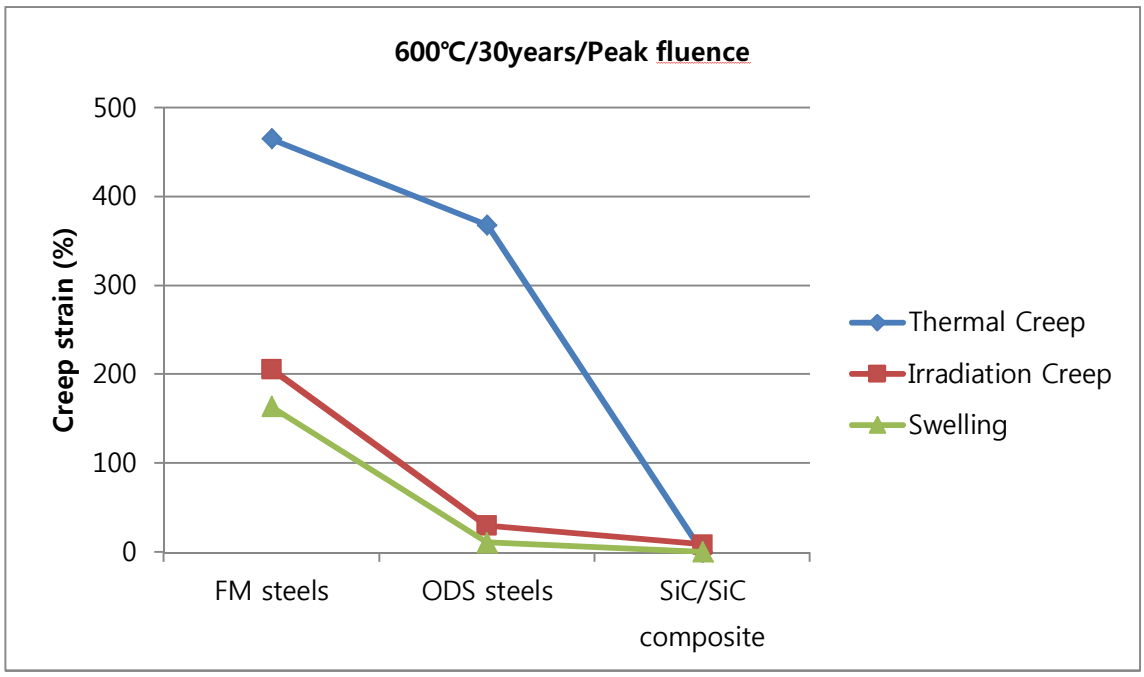

Fig 4.2 Comparing creep strain at 600℃/30years/Peak fluence

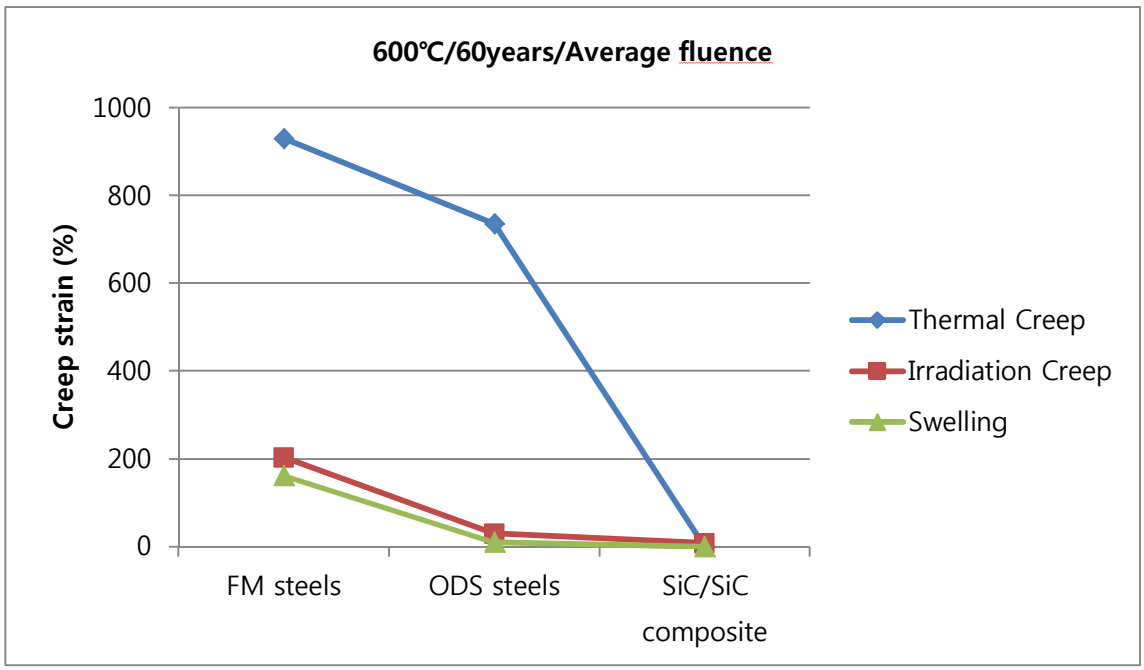

Fig 4.3 Comparing creep strain at 600℃/60years/Avg.fluence

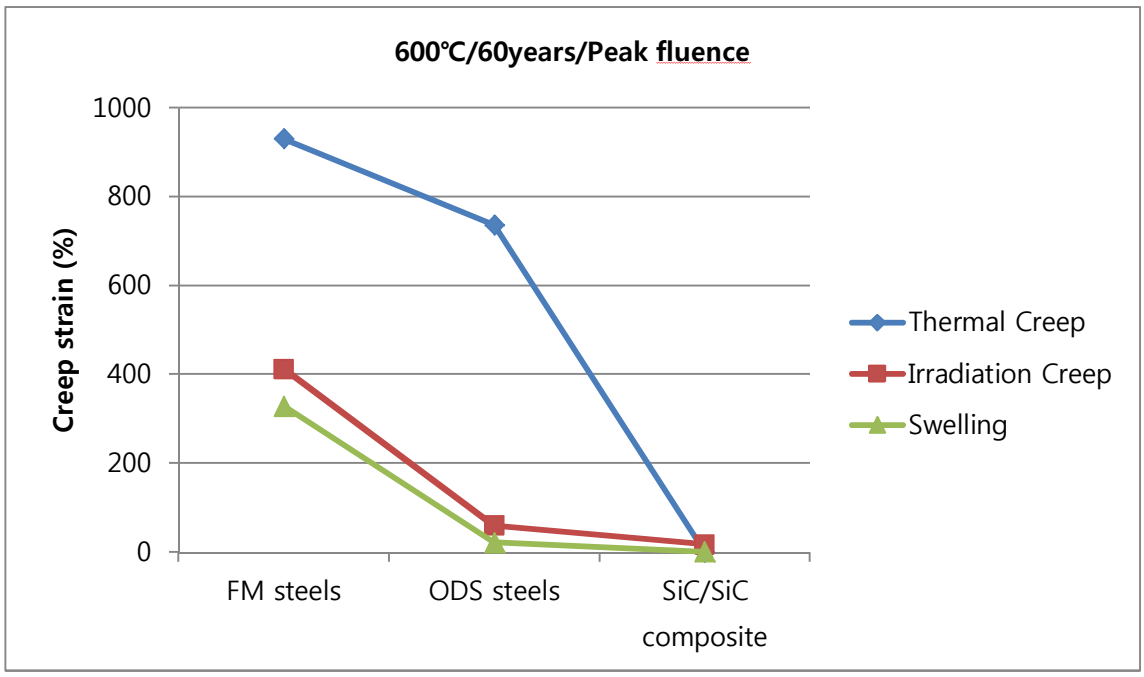

Fig 4.4 Comparing creep strain at 600℃/60years/Peak fluence

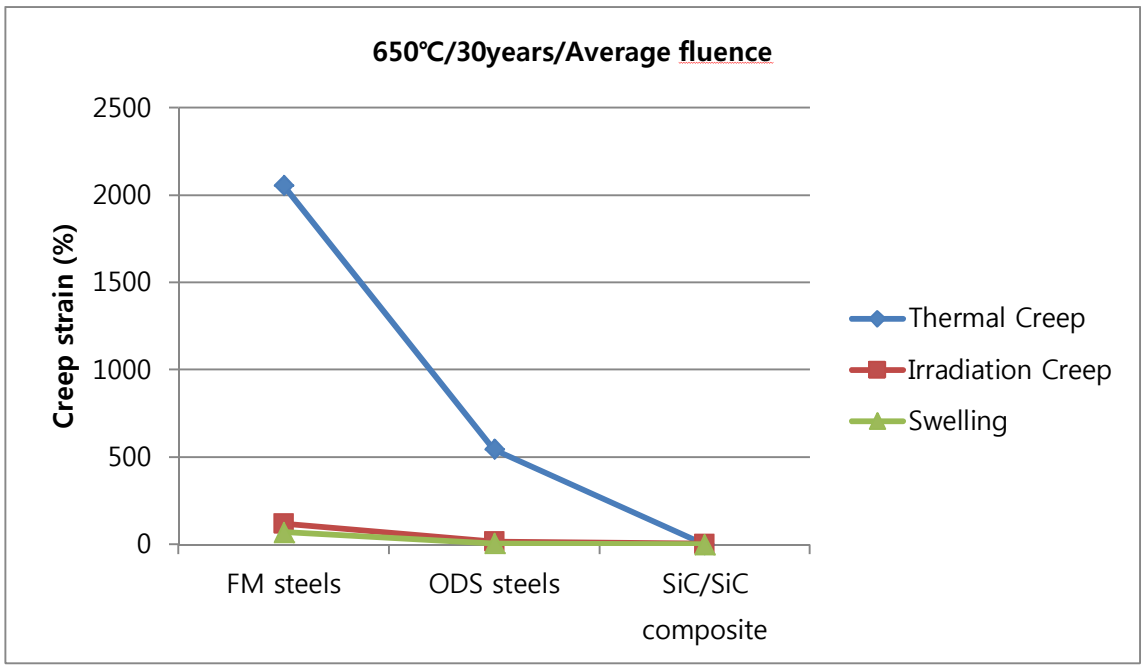

Fig 4.5 Comparing creep strain at 650℃/30years/Avg.fluence

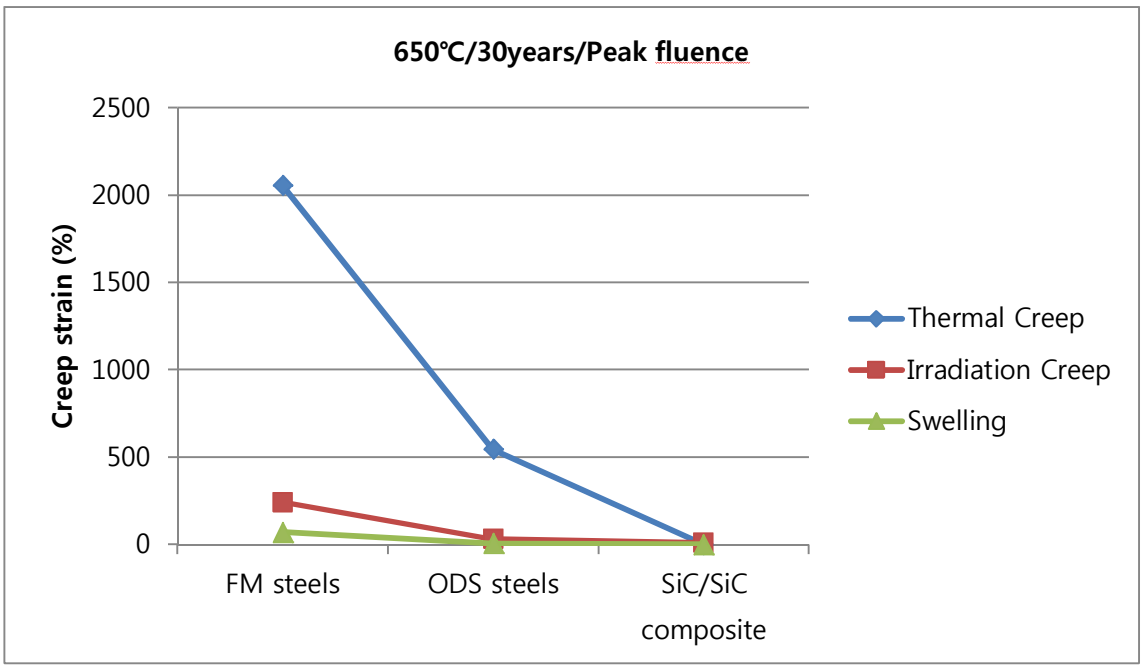

Fig 4.6 Comparing creep strain at 650℃/30years/Peak fluence

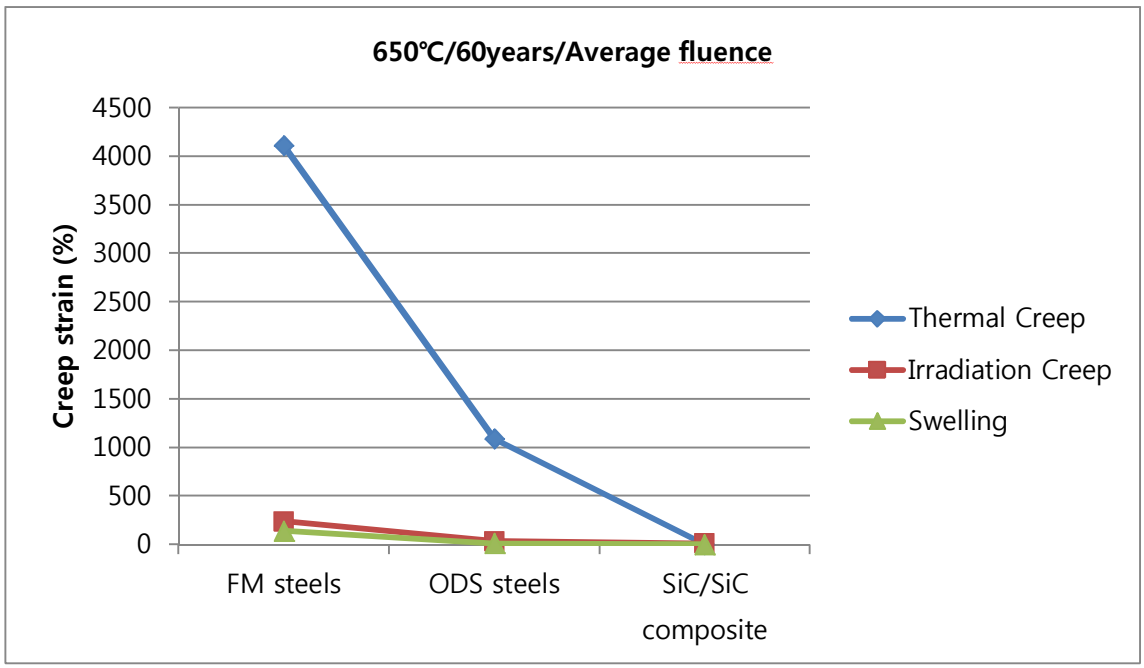

Fig 4.7 Comparing creep strain at 650℃/60years/Avg.fluence

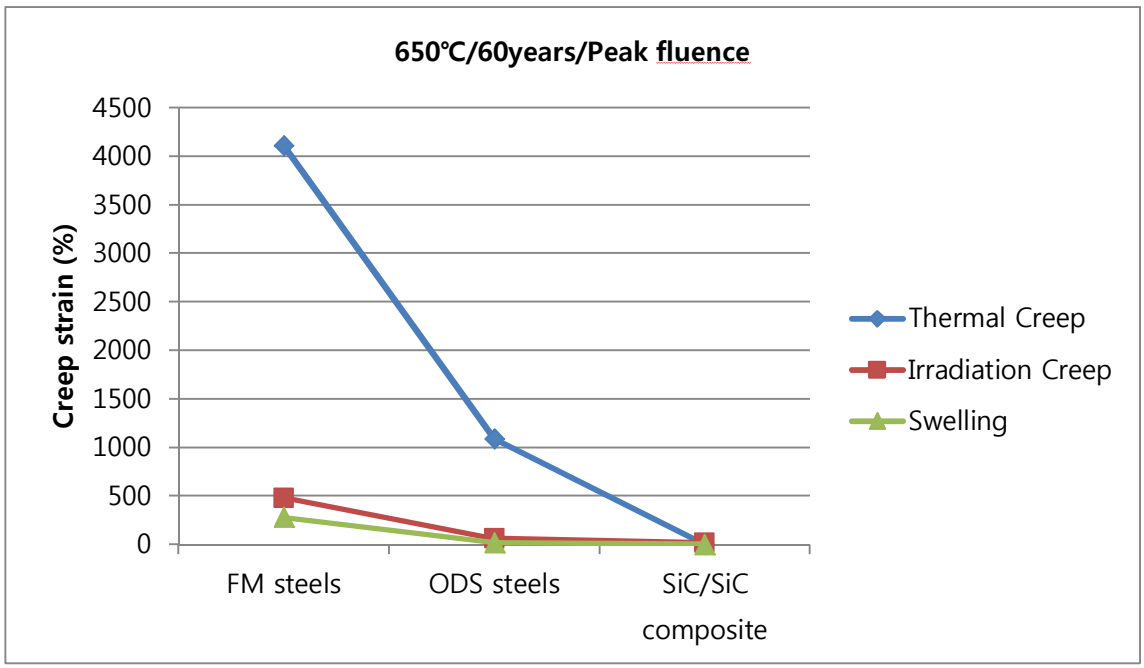

Fig 4.8 Comparing creep strain at 650℃/60years/Peak fluence

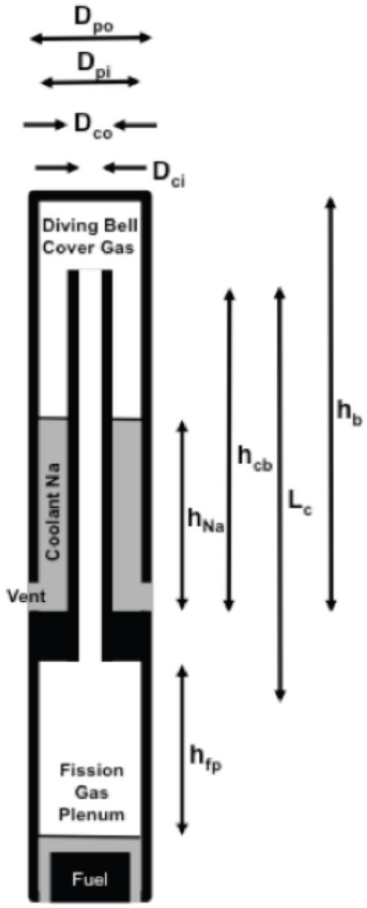

Fig 4.9 Illustration of Diving Bell Fuel Vent Concept with Relevent Dimensions Indicated [45]

V. Summary & Conclusion

The object of this research is to evaluate the performance of candidate cladding materials and to find a suitable material for UCFR cladding. The environment of UCFR is challenging for fuel, fuel cladding and structural materials. After screening candidate materials, the life prediction of fuel cladding is performed for UCFR environment. The most critical elements of design criteria are internal pressure, thermal creep, irradiation creep and swelling at life prediction. Theoretical and empirical models for key parameters of cladding materials are selected behaviors and used for the evaluations. As a result, SiC/SiC_f composite material can be used for UCFR cladding material at 30years, 600℃, average fluence. The use metal or alloy cladding for UCFR is needed, the vented fuel concept can be one of the options.

The preceding results show that UCFR environment (high temperature, high pressure and high irradiation strength) is too challenging environment for materials. As a results, the most possible concept of UCFR environment is 30y, 600℃, average fluence($2.29\times10^{24}n/cm^2$) among 8 concepts of UCFR environment. The others (FM steels, ODS steels) are not allowed in the aforementioned environment, only SiC/SiC_f composite is satisfied with the design. Therefore SiC/SiC_f composite can be used as UCFR cladding material. However, welding/joining of SiC/SiC_f composite need more experience and skills.

A study on theoretical model of cladding materials behavior needs to be pursued to improve existing models in the future. And the research of other design parameters such as fuel/cladding mechanical and chemical interaction affecting the life of UCFR cladding is also needed.

REFERENCES

1. T. K. Kim and T. A. Taiwo, "Feasibility Study of Ultra-long Life Fast Reactor Core Concept," *PHYSOR 2010*, May 9-14, (2010)

2. H. Sekimoto, K. Ryu, and Y. Yoshimura, "CANDLE: The New Burnup Strategy," *Nuclear Science and Engineering,* 139, pp.306-317 (2001).

3. Temitope A. Taiwo and Taek K. Kim, "Fuel Cycle Performance Characteristics of Advanced Once-Through Nuclear Energy Systems," *ICAPP2011*, Nice, France, May 2-5, (2011).

4. Charles Ahlfeld, et al., "Conceptual Design of a 500 MWe Traveling Wave Demonstration Reactor Plant," *ICAPP 2011*, Nice, France, May 2-5, (2011).

5. N. Ueda, et al., "Current Design Status of Sodium Cooled Super-Safe, Small and Simple Reactor," *ICONE 10*, Arlington, VA, April 14-18, 2002

6. DOHEE HAHN et al, CONCEPTUAL DESIGN OF THE SODIUM-COOLED FAST REACTOR KALIMER-600, NUCLEAR ENGINEERING AND TECHNOLOGY, VOL.39 NO.3 JUNE 2007

7. Masakazu ICHIMIYA, The Status of Generation IV Sodium-Cooled Fast Reactor Technology Development and its Future Project, Energy Procedia 7 (2011) 79–87

8. Ron Adamson et al, In-Reactor Creep of Zirconium Alloys, September 2009 Advanced Nuclear Technology International

9. R.L. Klueh et al, Ferritic/martensitic steels for next-generation reactors, 2007

10. G.Benamati et al, Mechanical and corrosion behaviour of EUROFER 97 steel exposed to Pb–17Li, 2002

11. R.L. Klueh et al, Tensile and creep properties of an oxide dispersion-strengthened ferritic steel, JNM, 2002

12. R.L. Klueh et al, Oxide dispersion-strengthened steels: A comparision of some commercial and experimental alloys, JNM, 2005

13. M.B. Toloczko et al, Irradiation creep of various ferritic alloys irradiated at ~400℃ in the PFR and FFTF reactors, 1998

14. Z. Jiao et al, Microstructure of helium-implanted and proton-irradiated T91 ferritic/martensitic steel, 2007

15. X. Jia et al, Microstructure in martensitic steels T91 and F82H after irradiation in SINQ Target-3, JNM, 2003

16. Yutai Katoh et al, Thermophysical and mechanical properties of near-stoichiometric fiber CVI SiC/SiC composites after neutron irradiation at elevated temperatures, 2010

17. L.L.Snead et al, Handbook of SiC properties for fuel performance modeling, JNM, 2007

18. Yutai Katoh et al, Current status and critical issues for development of SiC composites for fusion applications, 2007

19. Takanari Ogata et al, Analytical study on deformation and fission gas behavior of metallic fast reactor fuel, Journal of Nuclear Materials 230 (1996) 129-139

20. Chan Bock Lee et al, Fission gas release and swelling model of metallic fast reactor fuel, Journal of Nuclear Materials, 2001

21. Aydin Karahan et al, Modeling of Thermo-Mechanical and Irradiation Behavior of Metallic and Oxide Fuels for Sodium Fast Reactors, MIT-NFC-TR-110, August 2009

22. Y. Tsuboi et al, Mechanistic model of fission gas behavior in metallic fuel, Journal of Nuclear Materials 188 (1992) 312-318

23. Woan Hwang et al, Recent improvements in modeling fission gas release and rod deformation on metallic fuel in LMR, Annals of Nuclear Energy 27 (2000) 1059~1069

24. J. R. Hofmann et al, Internal Pressurization in Solid Mixed-Oxide Fuel Due to Transient Fission Gas Release, NUCLEAR SCIENCE AND ENGINEERING: 64, 713-723 (1977)

25. R. J. Amodeo et al, Constitutive design equations for thermal creep deformation of HT9, 1984

26. Lewis and Chuang, Constitutive thermal creep deformation relations for lifetime prediction of a fusion reactor first wall ferritic alloy, 1991

27. Ho jin Ryu et al, Thermal creep modeling of HT9 steel for fast reactor applications, 2011

28. A.Boltax et al, Void swelling and irradiation creep relationships, 1977

29. M.B. Toloczko et al, Irradiation creep of various ferritic alloys irradiated at ~400℃ in the PFR and FFTF reactors, 1998

30. J.E. FLINN et al, IN-REACTOR DEFORMATION OF SOLUTION ANNEALED TYPE 304L STAINLESS STEEL, 1977

31. John P. FOSTER et al, RESIDUAL STRESS MEASUREMENTS IN IRRADIATED SOLUTION-ANNEALED TYPE 304 STAINLESS STEEL TUBING, 1974

32. A. Boltax et al, Mixed carbide fuel pin performance analysis, 1974

33. Tae Woo Tak et al, PRELIMINARY DESIGN OF ULTRA-LONG CYCLE FAST REACTOR EMPLOYING BREED-AND-BURN STRATEGY, PHYSOR 2012 – Advances in Reactor Physics

34. W. B. GILBOY et al, A NEUTRON SCATTERING STUDY OF Fe56, Nuclear Physics 64 (1965) 130- 146

35. Alan E. Waltar et al, Fast Breeder Reactors, 1981

36. Robert J. Amodeo et al, Constitutive design equations for thermal creep deformation of HT-9, JNM, 1984

37. Wan Hwang et al, The Feasibility Study on Fuel Types for the KALIMER, 1997

38. A.J.Lovell et al, Predicted performance of the ferritic/martensitic alloy HT9 cladding in an FFTF test of advanced oxide fuel, 1983

39. F.A. Garner et al, Irradiation creep and swelling of the fusion heats of PCA, HT9 and 9Cr-1Mo irradiated to high neutron fluence, 1991

40. Garner F. A et al, Stress-enhanced swelling of metals during irradiation, 1981

41. Jianguo Wu et al, Storage Durability Life and Reliability Analysis of Welded Metal Bellows, Reliability, Maintainability and Safety (ICRMS) 2011 9th International Conference

42. Jin Sik Cheon et al, Sodium fast reactor evaluation: Core materials, Journal of Nuclear Materials 392 (2009) 324-330

43. F. Vitillo et al, A Vented Inverted Fuel Assembly Design for an SFR, Proceedings of ICAPP 2012

44. A. E. Wright et al, Development of Advanced Ultra-High Burnup SFR Metallic Fuel Concept – Project Overview, Transactions of the American Nuclear Society, Vol. 106, Chicago, Illinois, June 24–28, 2012

45. T. K. Kim et al, Fission Gas Venting for Ultra-high Burnup SFR Metallic Fuel Pin Design, Transactions of the American Nuclear Society, Vol. 106, Chicago, Illinois, June 24–28, 2012

46. A B ELAYDY and M HAFEZ, Influence of granular strontium chloride as additives on some electrical and mechanical properties for pure polyvinyl alcohol, *Bulletin of Materials Science* Vol.33 No.2 April 2010 pp.149–155

47. MB. Toloczko et al, Irradiation creep and swelling of the US fusion heats of HT9 and 9Cr-1Mo to 208 dpa at ~400℃, *Journal of Nuclear Materials*, 1994

Acknowledgements

First, Thanks to God, for everything in my life and for helping me to complete this work.

I would like to express my gratitude to all those who gave me the possibility to complete this thesis.

I am deeply indebted to my thesis advisor Professor Ji Hyun Kim whose help, stimulating suggestions and encouragement helped me in all the time of research for and writing of this thesis. And I owe special thanks to my thesis committee members, Professor Si Hwan Kim and Professor In Cheol Bang for their advice that helped me bring my research to final fruition.

My Lab. colleagues supported me in my research work. I want to thank them for all their help, support, interest and valuable hints. Especially I am obliged to Sang Hun Shin, Jong Jin Kim, Kyoung Jun Choi, Sang Il Choi, Seung Hyun Kim, Seung Won Lee, Sung Dae Park, Sarah Kang, Sung Man Kim, Han Seo, Byoung Jin Cho, Young Jin Kim, Tae Woo Tak, Dong Han You.

Thanks to my best friend, Hyung Ju Lee, Jae Hwan Park. Pray for each other forever!

Lastly, thanks to my family for their great support and help to accomplish this study. They are the cornerstone in my life.